Available online at www.sciencedirect.com
ScienceDirect
Tectonophysics 453 (2008) 211–232
TECTONOPHYSICS
www.elsevier.com/locate/tecto

Tectonic geomorphology of the easternmost extension of the Gulf of Corinth (Beotia, Central Greece)

Ioannis M. Tsodoulos [a,*], Ioannis K. Koukouvelas [a], Spyros Pavlides [b]

[a] Department of Geology, Division of Marine Geology and Geodynamics, University of Patras, Patras 26500, Greece
[b] Department of Geology, Aristotle University of Thessaloniki, Thessaloniki 54124, Greece

Received 20 November 2006; accepted 5 June 2007
Available online 9 February 2008

Abstract

The easternmost sector of the Gulf of Corinth, the Beotia area in Central Greece, is an area with active normal faults located between the two major rift structures of Central Greece, the Gulf of Corinth and the North Gulf of Evia. These active normal faults include WNW to E–W and NE to ENE-trending faults affect the landscape and generate basin and range topography within the Beotia. We study four normal fault zones and drainage basin geometry in the easternmost sector of the Gulf of Corinth to document the impact of active tectonics on the landscape evolution. Fault and drainage geometry are investigated based on detailed field mapping and high-resolution digital elevation models. Tectonic geomorphic analysis using several parameters of active tectonics provides information concerning the relative tectonic activity and fault growth. In order to detect areas of lateral stream migration that could indicate recent tectonic activity, the Transverse Topographic Symmetry Factor and the Asymmetry Factor are used to analyse drainage basin geometry in six large drainage basins and a drainage domain covering the study area. Our results show that vertical motions and tilting associated with normal faulting influence the drainage geometry and its development. Values of stream-gradient indices (S_L) are relatively high close to the fault traces of the studied fault zones suggesting high activity. Mountain-front sinuosity (S_{mf}) mean values along the fault zones ranges from 1.08 to 1.26. Valley floor width to valley height ratios (V_f) mean values along the studied fault zones range between 0.5 and 1.6. Drainage basin shape (B_S) mean values along the fault zones range from 1.08 to 3.54. All these geomorphic parameters and geomorphological data suggest that the analyzed normal faults are highly active. Lateral fault growth was likely produced by primarily eastward propagation, with the WNW to E–W trending faults being the relatively more active structures.

Keywords: Active normal faults; Fault segmentation; Geomorphic parameters; Range front geomorphology; Beotia in Gulf of Corinth; Beotia; Greece

1. Introduction

The understanding of active deformation and its significance for the long-term prediction of earthquakes has experienced remarkable progress through the study of geomorphology (Keller, 1986). The study of landforms that appear to be controlled by the interaction between tectonic and geomorphic processes is the focus of tectonic geomorphology (Mayer, 1986). Landscapes in tectonically active areas result from a complex integration of the effects of vertical and horizontal motions of crustal blocks and erosion or deposition by surface processes (Burbank and Anderson, 2001). As a consequence, geomorphic investigation in regions of active tectonics is a powerful tool for studies of tectonic geomorphology (i.e. Azor et al., 2002).

In regions of active extension, the presence of segmented normal faults is a common characteristic and plays an important role in the evolution of landscape (i.e. Gawthorpe and Hurst, 1993; Koukouvelas, 1998; Soliva and Benedicto, 2004). Furthermore, the segmented character of normal faults is a common feature of faults on all scales (Walsh et al., 2003; and references therein) and plays an important role in the development of normal faults throughout the interaction of their segments over time. Places of fault interaction and linkage processes are of great significance in seismology, petroleum geology, sediment accumulation and particularly to the landscape evolution.

* Corresponding author.
E-mail address: tsodoulo@upatras.gr (I.M. Tsodoulos).

0040-1951/$ - see front matter © 2008 Elsevier B.V. All rights reserved.
doi:10.1016/j.tecto.2007.06.015

The Aegean region (Fig. 1a) has experienced active extension since the Upper Miocene (McKenzie, 1972, 1978; Le Pichon and Angelier, 1979; Mercier et al., 1979; Angelier et al., 1982; Papazachos et al., 1984a,b; Boronkay and Doutsos, 1994; Jackson, 1994; Doutsos and Kokkalas, 2001). This extension is probably related to back-arc extension behind the Hellenic subduction zone and rotation of crustal blocks resulting from the dextral strike-slip motion on the North Anatolian Fault (Kokkalas et al., 2006 and references therein). In Central Greece, the extension is accommodated by the interplay between ENE and WNW-trending major active faults that affect the landscape, developing a Basin and Range type topography (Doutsos and Piper, 1990; Caputo and Pavlides, 1993; Roberts and Koukouvelas, 1996; Koukouvelas et al., 1999; Doutsos and Kokkalas, 2001) (Fig. 1b). Two of the most important rift structures within Central Greece are the Gulf of Corinth and the Northern Gulf of Evia (Fig. 1b) (Doutsos and Piper, 1990). The Gulf of Corinth is a 110-km-long active rift and is one of the fastest extending regions of the Earth's continental crust with up to 15 mm/a of N–S extension (Billiris

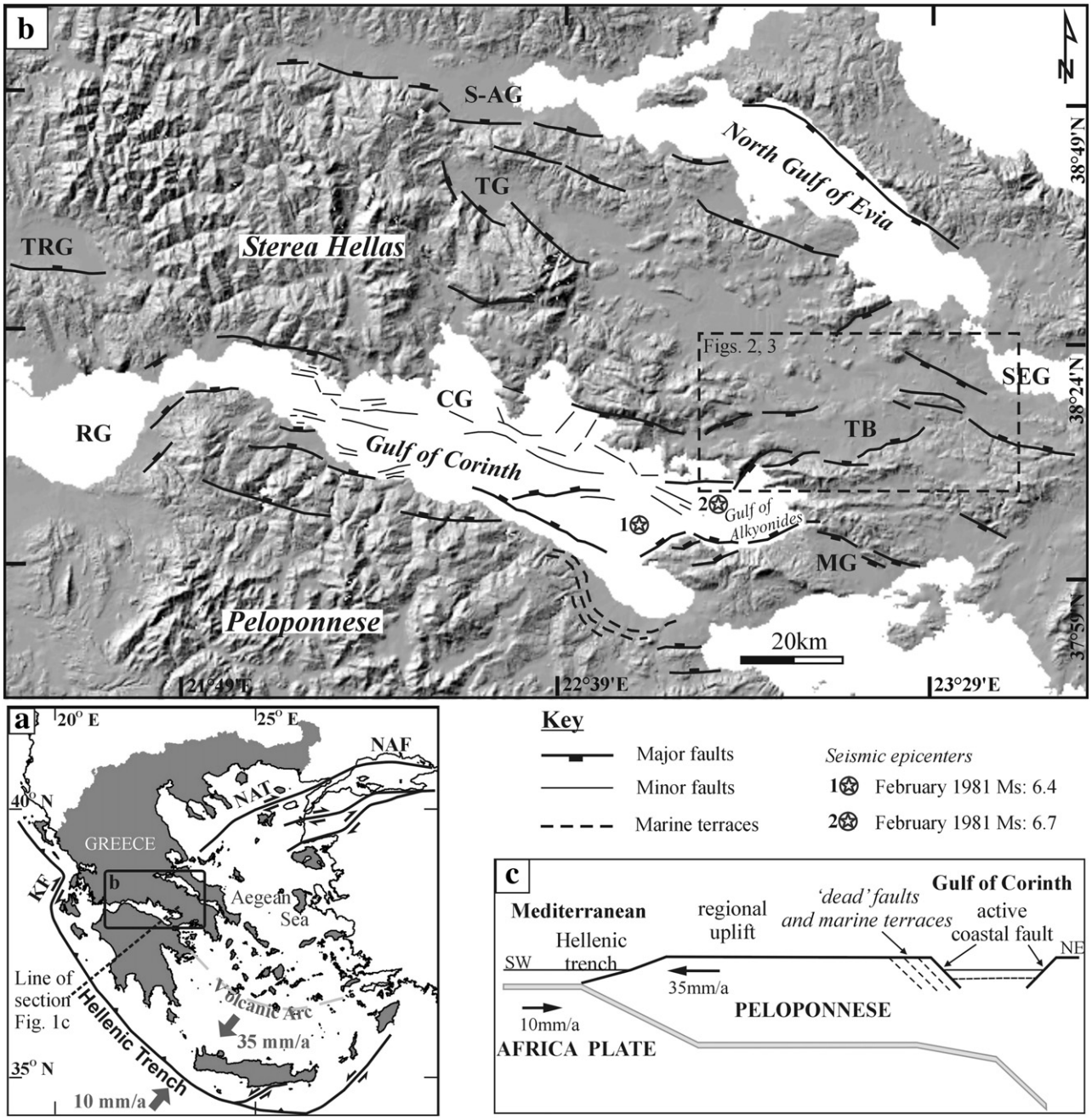

Fig. 1. (a) General map showing the main structural features of the Hellenic Arc and Trench system. KF: Kefallonia Fault; NAF: North Anatolian Fault; NAT: North Aegean Through. (b) Digital elevation model of the central Hellenic Peninsula showing the main structural features. CG: Corinth graben; MG: Megara graben; RG: Rio graben; S–AG: Sperchios–Atalanti graben; SEG: South Evia graben; TB: Thiva basin; TG: Tithorea graben; TRG: Trichonis graben. (c) Schematic section of the subducting Africa plate beneath Peloponnese and the Gulf of Corinth (modified from Leeder et al., 2003).

et al., 1991; Clarke et al., 1998; Davies et al., 1997; Briole et al., 2000). Extension across the Gulf of Corinth is accommodated by a system of segmented normal faults (Roberts and Koukouvelas, 1996; Koukouvelas et al., 1999; Micarelli et al., 2003; Pavlides et al., 2004). This segmentation is the dominant geometry for normal faults in the Gulf of Corinth (Koukouvelas and Doutsos, 1996). In particular, the easternmost sector of the Gulf of Corinth, where our study area is located, is an interesting area in terms of the moderate extension-rate (~10 mm/a) (Clarke et al., 1998; Briole et al., 2000) compared with the main Gulf of Corinth and the setting above the knee of the subducting Africa plate (Fig. 1c) (Hatzfeld et al., 2000; Leeder et al., 2003).

The Northern Gulf of Evia is a WNW–ESE trending fault system that can be traced all along the Sperchios Basin to the south coast of the Gulf (Fig. 1b) (Roberts and Jackson, 1991; Eliet and Gawthorpe, 1995; Goldsworthy et al., 2002). Extension-rate across the Northern Gulf of Evia is ~1 mm/a (Billiris et al., 1991). This extension is accommodated by a series of spectacular WNW-trending normal faults with footwalls ~1000 m high and abundant evidence of Holocene activity on scarps at their base (Jackson, 1999; Pavlides et al., 2004; Zovoili et al., 2004).

In Greece systematic studies of tectonic geomorphology are scarce except footwall topography analyses (Koukouvelas et al., 2001; Ganas et al., 2004) or some preliminary along fault

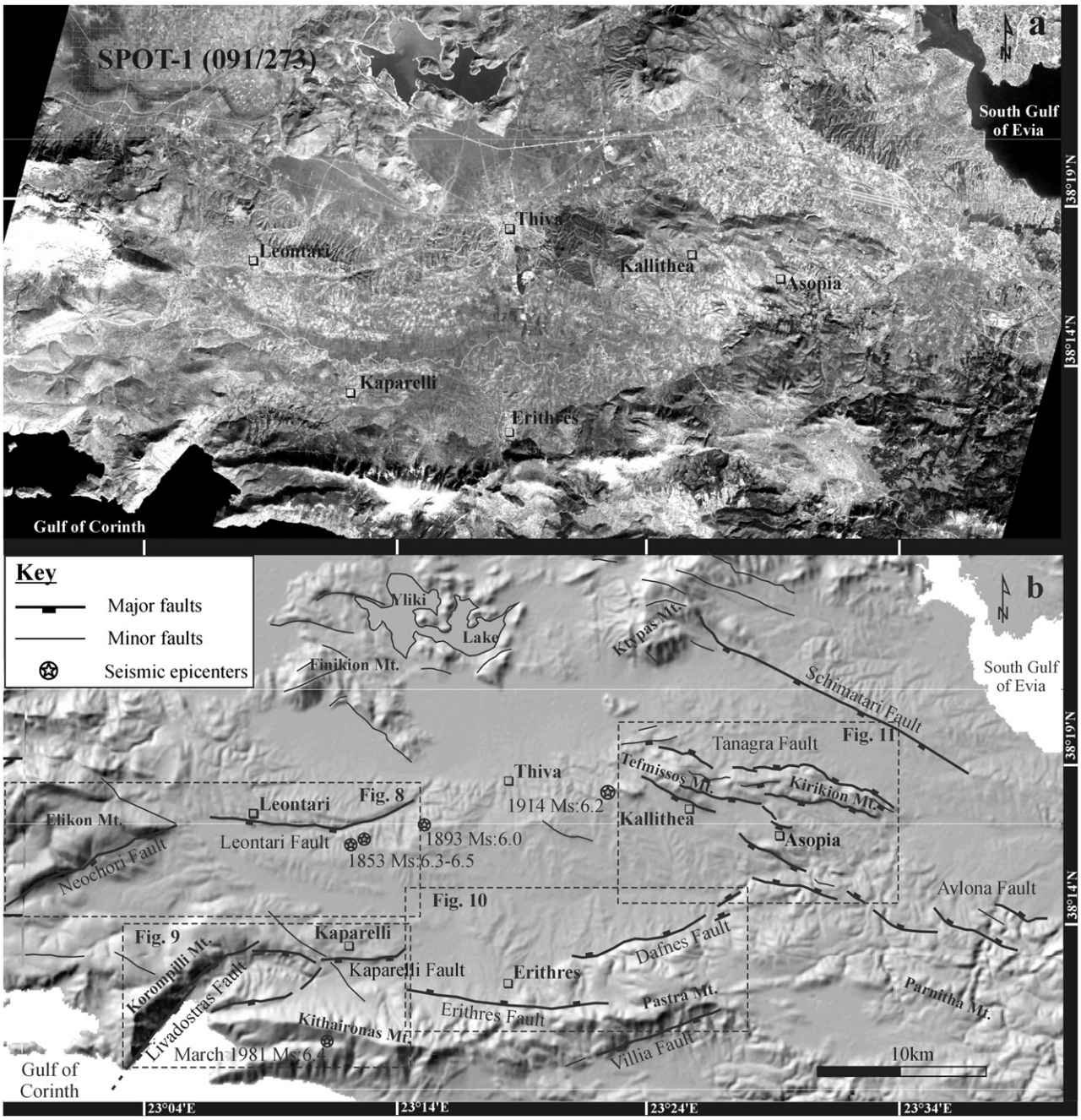

Fig. 2. Structural map of the easternmost sector of the Gulf of Corinth. (a) Satellite image of the study area. (b) Structural interpretation of (a), showing fault geometry overlain on the digital elevation model.

studies of the Valley Floor Width–Valley Height Ratio (V_f) index (Koukouvelas, 1998) and studies that examine the drainage pattern associated with active normal faults (Roberts and Jackson, 1991; Leeder et al., 1991; Eliet and Gawthorpe, 1995; Collier et al., 1995; Goldsworthy and Jackson, 2000; Pavlides et al., 2004).

The purpose of this study is to analyze the drainage pattern and landscape evolution in order to evaluate the tectonic activity and the fault growth within the actively deformed easternmost sector of the Gulf of Corinth (Fig. 2). Within the study area an array of strongly segmented faults that define basins is exposed allowing us to quantify the geomorphology between the two major rifts called Corinth and Evia. In order to achieve our aim, we used a variety of geomorphic parameters and detailed mapping of faults to refine geometry and evolution of fault systems in the study area. In addition, we used digital elevation models to estimate the geomorphic parameters. The use of digital elevation models permits the characterization and comparison of landscapes with a resolution and accuracy that is not possible to obtain from conventional topographic contour maps (Burbank and Pinter, 1999; Mayer, 2000). This analysis also shed light on the linkage of fault segments and the propagation of the studied basin-bounding faults.

2. Geology of the study area

The study area is located between the Gulf of Corinth and Evia Island, covering an area of approximately 2000 km^2 (Figs. 1 and 2). An array of normal faults has been mapped within the study area. The faults have a bimodal orientation distribution with WNW to E–W and NE to ENE-trend (Fig. 2). The most prominent basin in the study area is the Thiva Basin, bounded by major normal faults. In map view, the Thiva Basin is arcuate in shape and concave to the north. Its major axis trends between ENE, in the western part, and WNW in the eastern part (Fig. 3). The Thiva Basin contains two major intrabasin highs, the Korompilli–

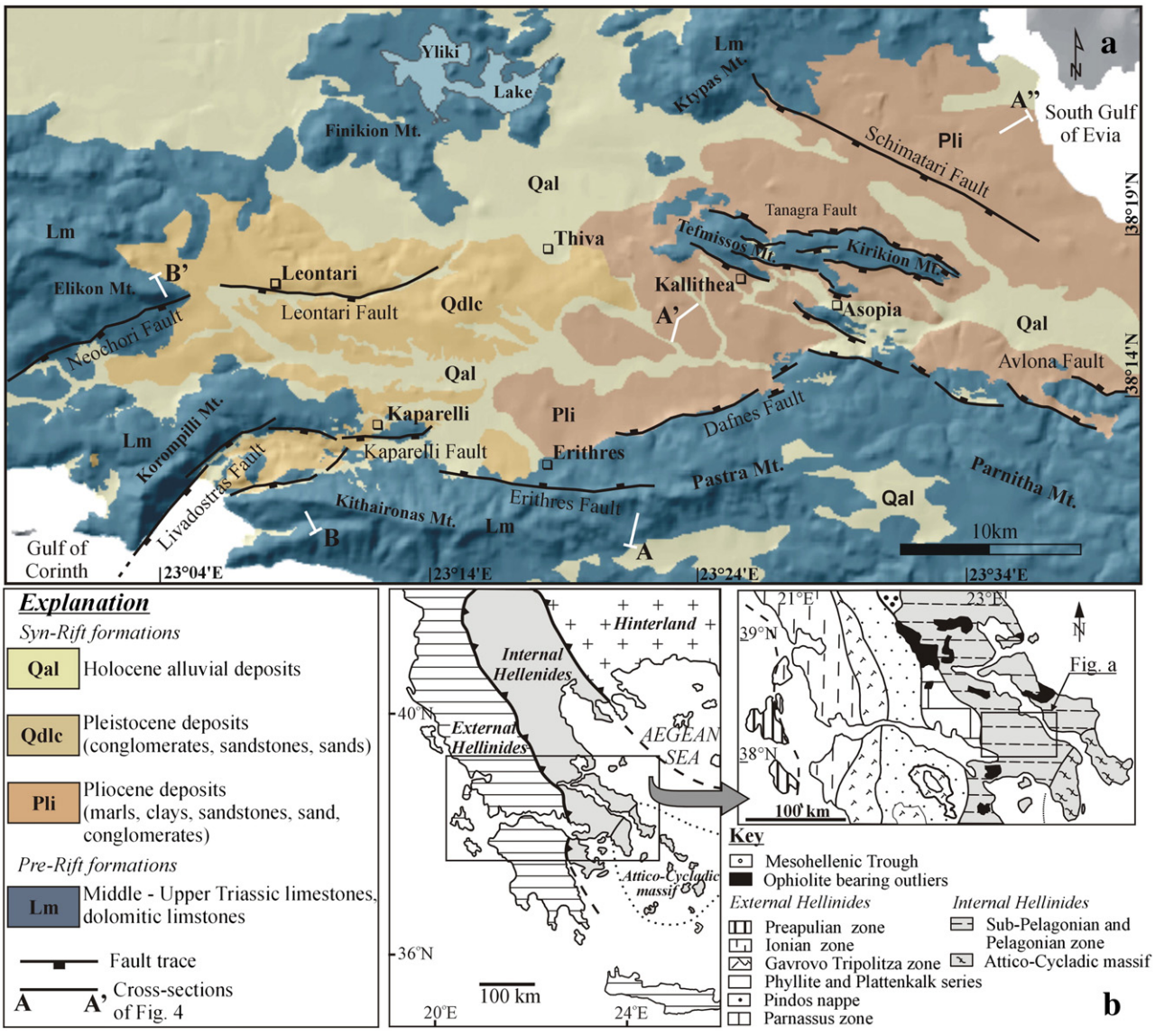

Fig. 3. (a) Simplified geological map of the study area. (b) Map of the Hellenides showing the isopic zones and significant structural elements.

Kaparelli range to the west and the Kallithea–Asopia range to the east (Figs. 3 and 4). Both intrabasin highs are fault controlled (Figs. 2 and 4).

The investigated area is located at the boundary between the Internal and External Hellenides. The pre-rift formations of the study area consist of pre-alpine and alpine formations that belong to the Sub-Pelagonian isopic zone of the Internal Hellenides (Fig. 3). The Sub-Pelagonian zone corresponds to the western slope of the Pelagonian microcontinent (Smith, 1977; Robertson et al., 1991). To the west, the External Hellenides comprises Mesozoic carbonate sequences called Pindos and Parnassos zones. The Pindos zone correspond to the Apulian passive continental margin while the Parnassos zone represents an Apulian-derived microcontinental fragment (Doutsos et al., 2006). Orogenic movements along the margin began in the Eocene and involved the eastward subduction of the Pindos Ocean beneath the Pelagonian continent (Doutsos et al., 1994, 2006; Degnan and Robertson, 1998). The pre-alpine formations within the Sub-Pelagonian zone are mainly composed of Upper-Palaeozoic shale, sandstones, greywacke, conglomerate and imbedded basic volcanic rocks (Renz, 1955; Dounas, 1971). Alpine formations of the zone and the study area consist of Middle–Upper Triassic to Low-Jurassic limestones and dolomitic limestones, deposited in a shallow water environment (Christodoulou, 1969).

The oldest known late- to post-orogenic sediments in the Thiva Basin include lacustrine marls and marly limestones, clays, sandstones and conglomerates of Serravallian age (~11.6 Ma) (Mettos et al., 2000). On top of the Upper Miocene sediments (and in conformity) a post-Miocene succession composed of fluvio-terrestial conglomerates, sandstones and sands was deposited (Dounas, 1971) (Fig. 3). The base of the fluvio-terrestial deposits consists of massive calcareous breccias. Holocene age alluvial deposits and recent scree compose the youngest sediments of the basin. However, it is important to note that the detailed post-Miocene stratigraphy in the area is in general poorly known.

According to the seismic catalogues the easternmost sector of the Gulf of Corinth has been affected by a series of strong earthquakes (Papazachos and Papazachou, 1997; Papadopoulos et al., 2000). Most of the recent seismicity in the study area is located in the southwestern sector between Kaparelli village and Kithaironas Mountain, and continues eastwards through the Thiva Basin (see also www.noa.gr). The study area has experienced at least seven destructive earthquakes over the last 300 years, where earthquake catalogues appear more complete (Fig. 2b). Two events of M_s 6.3 and 6.5 occurred in the Thiva region in 1853, during August and September respectively, causing extensive devastation of Thiva and the surrounding area (Ambraseys and Jackson, 1997, 1998) (Fig. 2). During the 1893 a strong earthquake of M_s 6.0 affected the area near Leontari village and is this event was considered to be hosted on the homonymous fault (Ambraseys and Jackson, 1990, 1997; Goldsworthy and Jackson, 2000). Another earthquake of M_s 6.2 which occurred during 1914 and caused severe damages in the broader area of Thiva, is apparently associated with the Kallithea–Asopia Fault zone (Ambraseys and Jackson, 1990). The last three well-studied strong earthquakes in the area occurred in 1981 (Jackson et al., 1982; Papazachos et al., 1984a,b; King et al., 1985; Pavlides, 1993). The first two events (M_s 6.4–6.7) occurred on February 1981 and caused extensive surface rupture along the southern coast of the Gulf of Alkyonides (Fig. 1), while the third event (M_s 6.4), occurred on March 1981, created surface ruptures along the Kaparelli Fault (Fig. 2).

3. Organization of the regional drainage system

The study area is divided into six main drainage basins and one domain (Fig. 5). The drainage basins are called hereafter

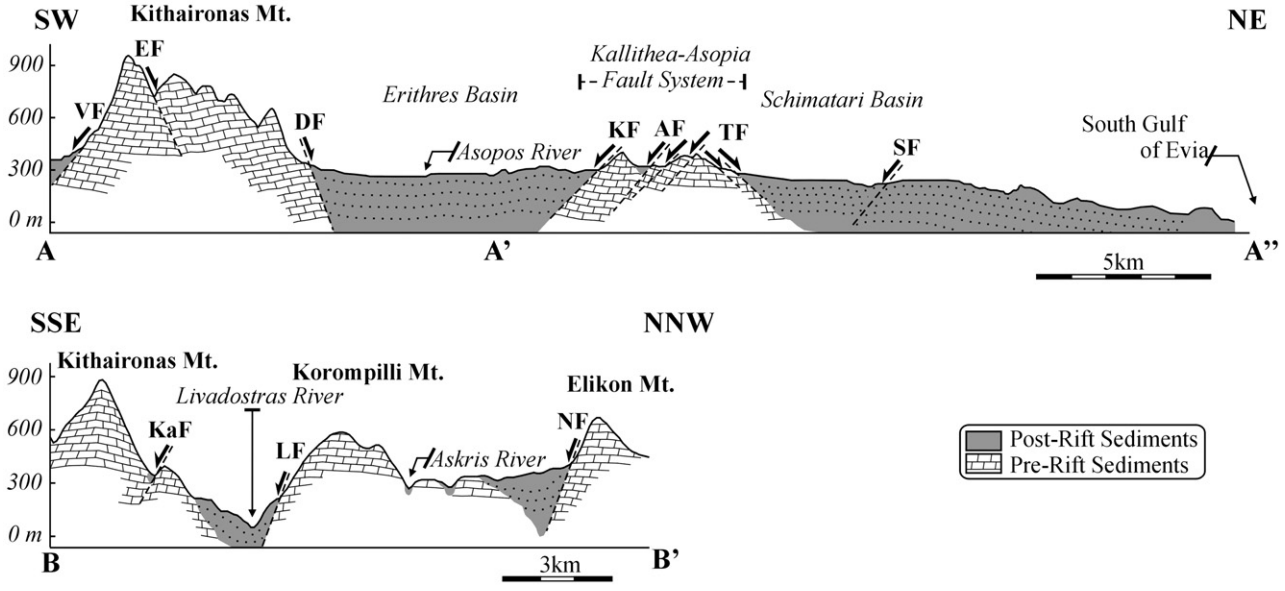

Fig. 4. Generalized geologic cross sections. See location in Fig. 3. VF: Villia Fault; EF: Erithres Fault; DF: Dafnes Fault; KF: Kallithea Fault; AF: Asopia Fault; TF: Tanagra Fault; SF: Schimatari Fault; KaF: Kaparelli Fault; LF: Livadostras Fault; NF: Neochori Fault.

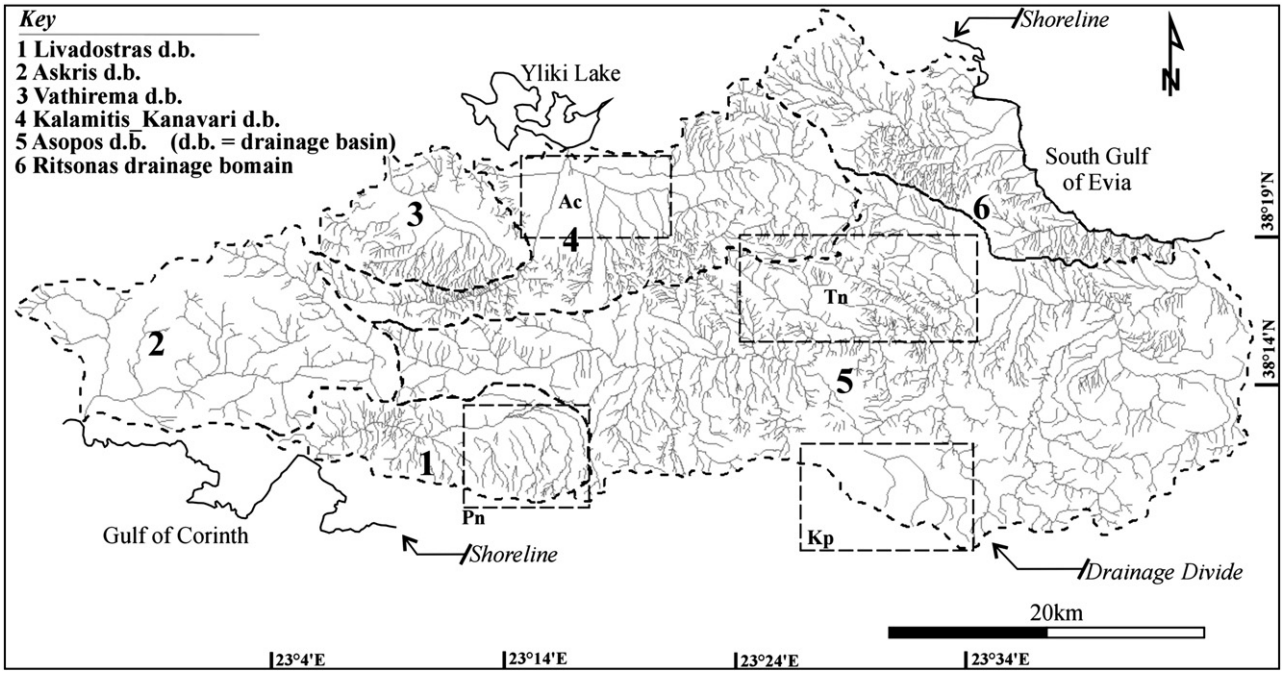

Fig. 5. Drainage map of the investigated area showing the divides between of the six major drainage basins and domain. Ac: Artificial channels; Kp: Karstic plain; Pn: Parallel network; Tn: Trellis network.

as: Livadostras, Asopos, Kalamitis–Kanavari, Vathirema and Askris (Fig. 5 and Fig. 6, drainage basins 1–5). In addition to the major drainage basins, a drainage domain is also defined. The Ritsonas drainage domain, named from the major river that runs along the domain, is defined as the area where the stream catchments that are broadly consistent in character, in terms of dimensions and their predominant direction of flow (Fig. 5, drainage domain). In general, except the effects of surface deformation and faulting on stream channel behavior, other factors as footwall rock type, climate and base-level changes can also affect the drainage and so it is important to isolate these secondary effects (Jackson and Leeder, 1994). The present-day climatic conditions in the area are characterized by a sub-humid Mediterranean climate dominated in summer by the Azores subtropical high-pressure cell, which gives rise to extended dry periods. In winter, the weather is wet, influenced by the southward displacement of the mid-latitude westerlies (Hilton, 1979; Barry and Chorley, 1998; Griffiths et al., 2002). The most significant effect of changing climate in the past is the fluctuation in water levels of lakes in the region. During the Quaternary, northeastern Central Greece included numerous lakes, with most important the Kopais Lake (now artificially drained), whose level fluctuated in response to changing climatic conditions. From pollen analysis of a sediment core from Kopais Lake, Okuda et al. (2001) suggest that lake water level was low during the glacial and relatively high during the interglacial periods. These base-level fluctuations could potentially have influenced the drainage. However in the studied range fronts, changes in base-level are inferred to have little or not effect on stream power and drainage. Drainage is thus incised where it coincide with faults. Although the floor of the main basins is mostly cultivated, some areas of natural vegetation still remain, especially in the mountainous areas. From the above data it is likely that not climatic or base-level changes affect the investigated drainage.

The Livadostras drainage is located in the southwest part of the study area and drains the southwesternmost part of the Thiva Basin (Fig. 5, drainage basin 1). The Livadostras River arises in the northern side of Kithaironas Mt. between villages of Plataies and Erithres and flows roughly in an east–west direction, to its mouth at the head of the Alkyonides Bay. Drainage pattern for the lower to the middle part of the basin is dendritic and becomes parallel for the upper part of the basin, probably affected by tectonic activity (Pn in Fig. 5).

A dentritic network that drains the south flanks of Elikon Mountain feeds the Askris River drainage basin, which is located in the western sector of the Thiva Basin (Fig. 5, drainage basin 2).

Vathirema drainage comprises a parallel drainage pattern (Fig. 5, drainage basin 3). Drainage in the southern side of this basin is characterized by a system of long, incised, sub-parallel streams that run northwards on the gentle slope of the uplifted footwall of the Leontari normal fault (Goldsworthy and Jackson, 2000). The Vathirema River drains at its middle and lower part the basin of a former strand of the Kopais palaeolake (Paraskevaidis, 1971; Okuda et al., 2001).

Kalamitis–Kanavaris drainage exhibits a more complex pattern (Fig. 5, drainage basin 4). Kalamitis River is fed by a dendritic network, which drains the northeastern part of the basin. It flows to an east–west direction and reach Yliki Lake. Kanavari River mainly runs parallel to the Leontari fault up to the confluence with the Kalamitis River. It is fed by a sub-parallel system of rivers that run down the dipping slope of the Leontari fault footwall block. Kalamitis–Kanavaris drainage basin at its lower part is at present modified by a system of irrigation channels (Ac in Fig. 5).

The Asopos drainage is the largest drainage basin within the study area and is strongly influenced by the relief and tectonic gradients produced by a series of normal faults (Fig. 2 and 4). Both axial (E–W trending) and lateral (N–S trending) drainage systems are developed (Fig. 5, drainage basin 5). Axial drainage is dominated by the Asopos River and is fed by a dendritic network that drains almost the entire southern part of the Thiva Basin. Drainage throughout the basin is predominantly dendritic, although clear examples of trellis drainage networks are found to the north of the basin (Tn in Fig. 5), within the uplifted Kallithea–Asopia Fault zone. In contrast, to the lateral and axial drainage systems throughout the major part of the basin, a discrete area of drainage located in the southern part of the basin drains a karstic plain (Kp in Fig. 5).

Finally, the Ritsonas drainage domain (Fig. 5 drainage domain 6) includes several small drainage basins one of which is the Ritsonas River drainage basin. The Ritsonas River drainage basin is the largest drainage basin within the domain. The reason that we found it useful to define this domain is the common drainage basin characteristics of all the rivers included in this domain. In the central part of this domain, the drainage occurs on a dipping surface that gently descends to the NE. This slope and its superimposed drainage directions are the result of the action of the SW dipping Schimatari normal fault. Drainage pattern throughout this domain is mainly dendritic, except some places that exhibit a parallel character.

4. Methodology of morphometric analysis

The estimate of morphometric parameters (geomorphic indices) requires for more accurate results a high-resolution digital elevation model. A variety of techniques can be used in order to construct DEMs. Among them digitizing topographic contours from existing topographic maps and spaced gridded data derived from digital photogrammetry techniques based on stereo satellite images or aerial photographs (Mayer, 2000). In our case a DEM for the study area was obtained by digitizing topographic contours from 1:50,000 scale topographic maps, supplied from the Hellenic Army Geographical Service (HAGS), with vertical accuracy of 10 m. In order to imprint in detail morphometric parameters, of specific sites of the study area, we acquired stereo-pairs of aerial photographs at an average scale of 1:15,000. Detailed DEMs with grid resolution of 5 m were constructed using digital photogrammetric techniques. Shaded relief images were also used, derived by processing DEMs following the method of Yoeli (1965), because they represent a very powerful tool for the assessment of the structural setting of a region giving particular emphasis into the morphological features (Onorati et al., 1992). For the purposes of this study, we extracted the morphometric properties from the DEMs using standard GIS methods.

4.1. Drainage basin asymmetry

To reveal possible patterns of ground tilting in the study area we used two quantitative morphometric methods (Fig. 6). These are the Transverse Topographic Symmetry Factor (T) following the basic technique presented in Cox (1994) and Cox et al. (2001) and the Asymmetry Factor (AF) which is described in Keller and Pinter (2002).

The Transverse Topographic Symmetry Factor is defined as a ratio

$$T = D_a/D_d,$$

where D_a is the distance from the stream channel to the midline of its drainage basin (measured perpendicular to a straight line segment fit to the channel), and D_d is the distance from the basin margin (divide) to the midline of the basin. If the stream is in the middle of its drainage basin, then $D_a=0$ and the ratio $T=D_a/D_d=0$ (a symmetrical drainage basin) (Fig. 6a). As the stream migrates laterally away from the center of the basin and toward one of the two margins, the value of T increases and approaches 1. In order to calculate the T index the main stream of Asopos River was divided into 1 km-long segments and its main tributaries (forth order) and all the other rivers that analyzed were divided into 0.5 km segments. The values of T are calculated for each segment and represented as a two-dimensional vector. The length of the vector is equivalent to the ratio D_a/D_d, and its direction is perpendicular to the segment of the stream. The vector direction indicates movement of the segment, in the following sense and for the river, with regard to the basin midline (Fig. 6a and b). Statistical analysis of the calculated vectors was used to estimate the most prominent direction of stream migration, the magnitude and a measure of dispersion. In a set of vectors, the most dominant direction can be found by calculating the resultant vector (Davis, 2002). The direction of the resultant vector is the mean direction (θ) of all the calculated vectors. The length of the resultant vector divided by the number of the calculated vectors gives the mean resultant length (R), which is a measure of dispersion (Davis, 2002). The mean resultant vector length ranges from zero to one, values of R near one indicate small dispersion of the observation, while values near zero indicate that the vectors are widely dispersed. This method can give a quantitative description of mean transverse topographic basin symmetry and highlight whether external forces (predicting preferred asymmetry) or internal fluvial processes (predicting random asymmetry) give rise to basin asymmetry in a given area (Cox, 1994). This method has been applied by Cox (1994), Cox et al. (2001) and Garrote et al. (2006) for the southwest and southeast Mississippi Embayment and from Salvany (2004) for the Guadiamar basin, where the asymmetry of the drainage basins was interpreted as the result of tectonic tilting.

The Asymmetry Factor can detect tectonic tilting on drainage basin scales or large areas and is sensitive to tilting perpendicular to the direction of the trunk stream. It is defined as,

$$\mathrm{AF} = 100(A_r/A_t),$$

where A_r is the area of the basin on the right to the river flow, and A_t is the total area of the drainage basin. Values of AF greater or less than 50 may suggest tilt. The Asymmetry Factor was applied to draw conclusions on tectonically induced tilting in the Nicoya Peninsula by Hare and Gardner (1985) and in the Guadiamar basin by Salvany (2004).

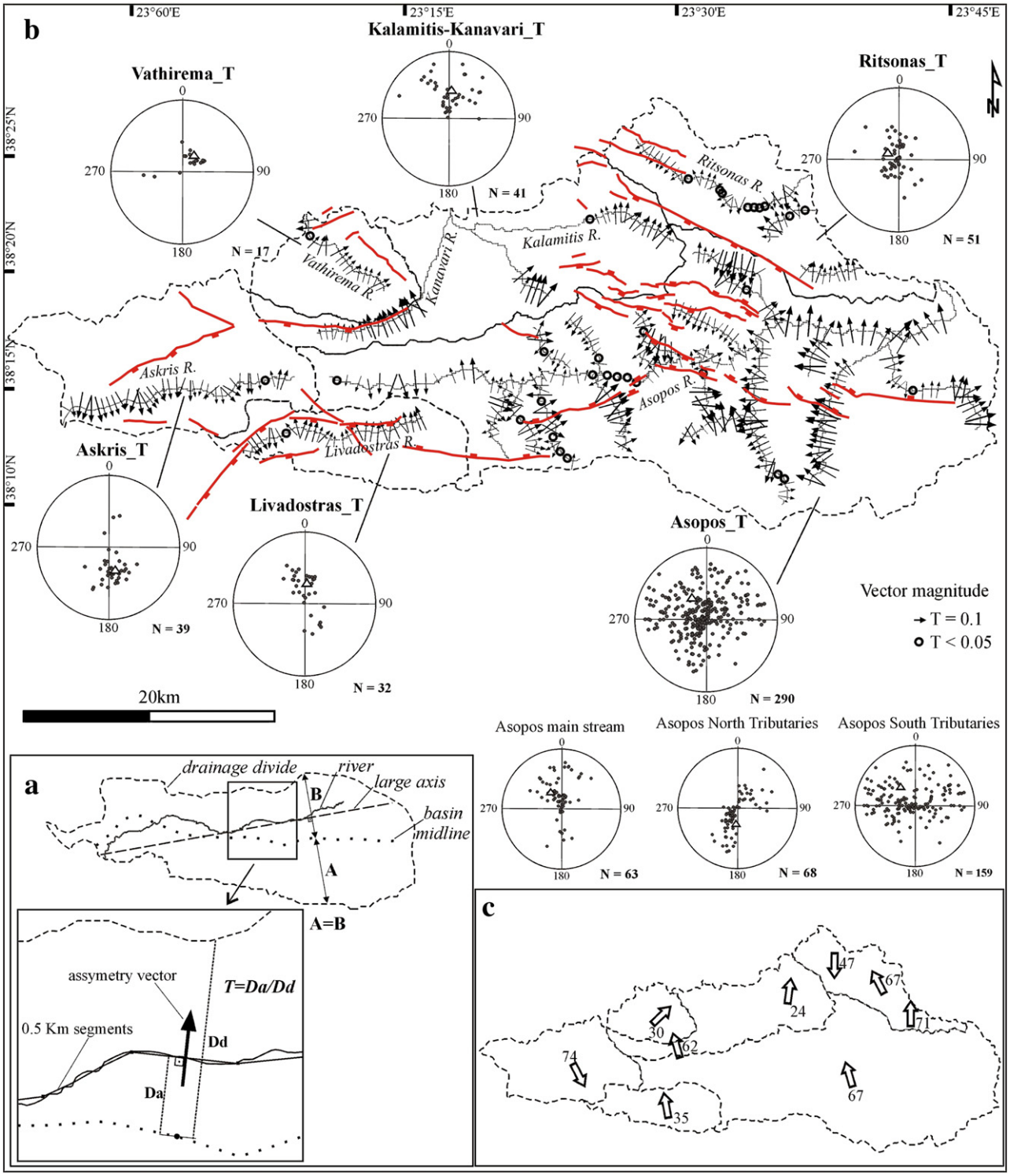

Fig. 6. (a) The Transverse Topographic Symmetry method proposed by Cox (1994) (modified from Salvany, 2004). (b) The basin asymmetry vectors within the investigated area. Polar plots of asymmetry vectors. At center, magnitude = 0; at margin magnitude = 1. Triangles indicate the mean vector. (c) Asymmetry Factor values and direction of tilt for the studied drainage basins.

4.2. Basin asymmetry results

The Transverse Topographic Symmetry Factor method was applied to the five drainage basins and the drainage domain of the study area. The Livadostras, Vathirema and Kalamitis–Kanavari drainage basins are characterized by N–NE migration of their principal streams, as suggested by the mean direction of the resultant vectors (Fig. 6b). The mean values for *T* are 0.33, 0.30 and 0.43, respectively. The *R* value of the Livadostras and Vathirema drainage basins shows a medium dispersion, while

for the Kalamitis–Kanavari drainage basin a small dispersion of *T*-vectors is observed. In Kalamitis–Kanavaris drainage basin the western tributary (Kanavari R.) displays NW-oriented *T*-vectors as an exception of the general trend of the basin mean direction. For the Kalamitis–Kanavaris drainage basin we calculated only the upstream vector segments because the downstream part of the mainstream has been modified by the construction of irrigation channels.

In the western part of the study area, the mean value of the *T*-vector for the Askris drainage basin is 0.37. The data are concentrated in the southeast quadrant of the polar plot and agree with the southeastward migration suggested by the asymmetry of the principal river basin. The mean resultant length for Askris drainage basin is 0.78 showing a small scatter of the vectors. This suggests that Askris River has migrated uniformly to the SE.

The Ritsonas drainage domain is located in the eastern part of the study area with a T-vector mean value of 0.25 and a mean direction 308°. The Ritsonas River itself has a mean value of the *T*-vector of 0.17 showing a southward mean direction of migration while the other two studied rivers show a *T*-vector value of 0.29 and a NNW direction of migration.

In the Asopos drainage basin, the mean value of the *T*-vectors for all the analysed rivers of the basin is 0.39 with an azimuth of 326° (Table 1). The Asopos River itself has a mean value of the *T*-vector of 0.35 showing a NW mean direction of migration, and a small dispersion of the vectors as suggested by the mean resultant length (0.78). The Asopos tributaries that are located at the northern side of Asopos mainstream display S–SW and NE-trending *T*-vectors directions. The mean direction is S–SW and the mean value for *T* is 0.32. The Asopos northern tributaries have widely dispersed vectors ($R=0.32$). The Asopos southern tributaries, are located at the southern side of Asopos, display a NW direction of the mean vector with a mean value of 0.43. They also show a tilting within the footwall of the Erithres–Dafnes Fault zone.

As proposed by Cox (1994) and Cox et al. (2001) following the methodology of Curray (1956), for the analysis of two-dimensional vector data, the level of statistical confidence of a mean vector can be stated as:

$$p = e^{(-L^2 n)(10^{-4})},$$

where p is the probability of obtaining a greater mean vector magnitude by change combination of random vectors, L is the mean vector magnitude multiplied by 100, and n is the number of observations. For the data presented in Fig. 6, the probability that the basin vectors are random is $p<0.05$ except Vathirema drainage with value of $p=0.2$ (Table 1).

The Asymmetry Factor displays a wide range of values (Fig. 6c and Table 1). The AF of Asopos, Livadostras, Kanavari and the two subbasins of Ritsonas domain show a general trend of uniform tilting to the NNW. The AF values of Vathirema and Kalamitis basins have similar low values showing a general trend of uniform tilting to the NNE. However, Askris and Ritsonas rivers do not follow this tendency. Askris shows a tilting to the SE, while the AF value of Ritsonas suggests a symmetric pattern rather than a tilting geometry.

Table 1
Morphomatric parameters of drainage basins

Drainage basin	Surface area	Asymmetry Factor	Transverse Topographic Symmetry Factor			
	A (km^2)	AF (%)	T	Bearing	R	p
1. Livadostras	100	35	0.33	2°	0.55	0.03
2. Askris	197	74	0.37	168°	0.78	<0.01
3. Vathirema	81	30	0.30	25°	0.60	0.2
4. Kalamitis–Kanavari	233	24/62	0.43	5.1°	0.88	<0.01
5. Asopos	711	67	0.39	326°	0.20	<0.01
6. Ritsonas	151	47/67/71	0.25	308°	0.19	0.04

T: mean vector magnitude.
R: mean resultant vector length (dispersion).
p: probability that drainage vectors are random.

Rivers controlled completely by faults are strongly asymmetrical, i.e. Leontari Fault that appears to control the Kanavari River. Stronger asymmetry is due to large isolated faults. Position of the fault within the basin is also important. For example, the Erithres and Dafnes Faults cross in the middle the Asopos basin. In this case, the basin river appears symmetric although it is obvious that the river was captured by the fault.

4.3. Stream length-gradient index

The stream length-gradient index (S_L) (Hack, 1973) is sensitive to channel slope changes, allowing the evaluation among possible tectonic activity or rock resistance (Keller and Pinter, 2002; Azor et al., 2002). This index is calculated for a particular reach of interest and it is defined by Keller and Pinter (2002) as:

$$S_L = (\Delta_H/\Delta_L)L,$$

where Δ_H/Δ_L is the channel gradient (slope) of the reach with Δ_H assign as the difference in elevation between the upper and the lower part of the reach, Δ_L the length of the reach and L is the total channel length from the point of interest (middle of the reach) where the index is being calculated upstream to the highest point of the channel. All streams and major tributaries in the study area have been analyzed and the S_L index calculated for about 4150 points covering the study area. A convenient interval of 20 m was selected as Δ_H. The values of the index at the most distant stream reaches may include significant error (Keller and Pinter, 2002), so index was not estimated for the last two uppermost reach. In order to visualize the spatial point pattern of the calculated index value we constructed a density map of the S_L index (Fig. 7).

The S_L index density map in Fig. 7 was constructed using Kernel estimation method. According to the Kernel estimation of the density of a parameter, points that fall within a circular search area are summed and then divided by the search area size to get each cell's density. The points lying near the center of a raster cell's search area are weighted more heavily than those lying near its edge. The result is a smoother distribution of values. The radius of the search area was 1250 m and the cell's size 50 m^2.

Fig. 7 shows that the areas of anomalously high values of S_L are primarily located along the studied faults.

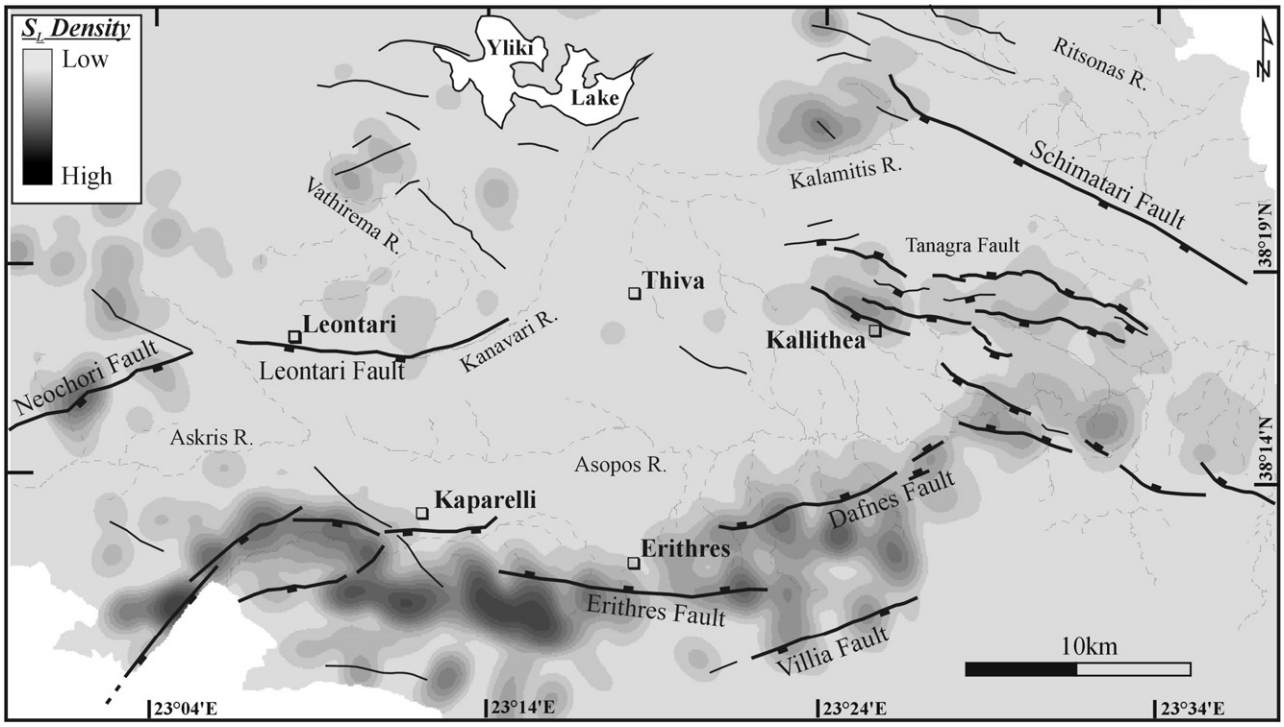

Fig. 7. Density map of stream length-gradient index (S_L) within the investigated area.

4.4. Mountain-front sinuosity

The mountain-front sinuosity index (S_{mf}) (Bull and McFadden, 1977) is defined as

$$S_{mf} = L_{mf}/L_s,$$

where L_{mf} is the length of the mountain front along the mountain-piedmont junction and L_s is the straight-line length of the mountain front. Mountain-front sinuosity index reflects the balance between the tendency of erosion to produce an irregular or sinuous mountain front and active tectonics that tends to produce a relatively straight mountain front, coincident with an active range-bounding fault. Low values of S_{mf}, near 1.0, indicate relative straight mountain fronts associated with high tectonic activity at this particular front. The S_{mf} value increases if the rate of uplift is reduced or ceases and erosional processes start to produce a sinuous mountain front that becomes gradually more irregular. High values of S_{mf} (>3.0) characterize mountain fronts that are so modified by erosional processes that the range-bounding fault initially responsible for the mountain front formation may be more than 1 km away from the present erosional front (Bull and McFadden, 1977). The investigated fronts were subdivided along strike into discrete segments with similar geological and morphological characteristics based on the following assumptions: a) intersection with cross-cutting major drainages, b) abrupt changes in lithology, c) changes in mountain front orientation, and d) abrupt changes in the major morphological characteristics of the mountain front relative to adjoining front segments, as proposed by Wells et al. (1988). In order to calculate the mean S_{mf}, five different digital values of L_{mf} values measured in the DEM, and the reported data are the mean values for each range front (Silva et al., 2003).

4.5. Valley Floor Width–Valley Height Ratio

The Valley Floor Width–Valley Height Ratio (V_f) indicates whether a stream is actively incising creating V-shaped valleys, as a response to active uplift, or is primarily eroding laterally creating broad-floor valleys (U-shaped) correlated with low rates of uplift. It is calculated as:

$$V_f = 2V_{fw}/[(E_{ld} - E_{sc}) + (E_{rd} - E_{sc})],$$

where V_{fw} is the width of the valley floor, E_{ld} and E_{rd} are the elevations of the left and right valley divides, respectively, and E_{sc} is the elevation of the valley floor (Bull and McFadden, 1977). In this study, transverse valley profiles for determining V_f were located ~250 m upstream from the mountain front in smaller drainage basins, and in large drainage basins transverse valley profiles were located ~250 and ~500 m upstream from the mountain front following Ramirez-Herrera (1998). High values of V_f characterize low tectonic activity valleys, while low V_f values characterize actively incising valleys. The V_f values were calculated for the most important canyons (rivers, valleys) along the studied mountain fronts. The Valley Floor Width–Valley Height Ratio was applied by many researchers (Bull and McFadden, 1977; Koukouvelas, 1998; Ramirez-Herrera, 1998; Zuchiewicz, 1998; Azor et al., 2002; Silva et al., 2003) in order to identify tectonically active fronts.

4.6. Drainage basin shape

Basins with elongated shapes characterize active mountain range areas while after cessation of mountain uplift their shapes became more circular (Bull and McFadden, 1977). Drainage basin shape (B_s) is an elongation ratio and describes the planimetric shape of a basin. It is expressed as:

$$B_s = B_l/B_w,$$

where B_l is the length of the basin, measured from its mouth to the most distal point in the drainage divide, and B_w is the width of the basin measured across the short axis defined between left and right valleys divides (Ramirez-Herrera, 1998). The index depicts differences between elongated basins with high values of B_s, and more circular basins with low values. The drainage basin shape was calculated for the drainage basin of streams that cross the major studied faults.

5. Geomorphic setting along the range-front fault zones

Along-strike displacement profiles were surveyed on fault segments within the study area. All individual profiles increase to a maximum displacement (Dmax) somewhere within the fault trace and decrease to displacements close to zero at the tips. Beyond these general characteristics, displacements profiles show a wide variety of shapes and many of them show significant asymmetry. Some profiles show larger scale irregularities and multiple linkage and interaction (Peacock and Sanderson, 1991; Scholz et al., 1993; Cartwright et al., 1995; Dawers and Anders, 1995). The footwall topographic profile, extracted from the digital elevation model, follows the crest of the uplifted footwall, while the hanging-wall topographic profile runs along the alluvial surface near the fault trace. When these topographic profiles are plotted together, they define the observable relief across the fault. Relief represents a minimum estimate of vertical displacement, because erosion might have lowered the uplifted crest and deposition of unknown thickness has certainly occurred in the hanging-wall block.

Drainage basins have considerable persistence as geomorphic landscape elements and so they can provide insights on the long-term evolution of the landscape (Burbank and Anderson, 2001). Footwall drainage basins geometries of the studied faults can reveal useful information of fault activity, growth and evolution.

We focused our research on four fault zones, which are described from west to east: the Neochori–Leontari, the Livadostras–Kaparelli, the Erithres–Dafnes and the Kallithea–Asopia fault zones. We restricted our study on these faults zones because they are the longer within the study area, their relief is in the order of >100 m, most of them host strong earthquakes and finally they appear to exert strong control on the drainage pattern.

5.1. Neochori–Leontari Fault zone

The Neochori–Leontari Fault zone at the western part of the study area includes two prominent segments called hereafter as the Neochori and Leontari Faults (Fig. 8). Both of them are south-dipping normal faults. The Neochori fault is ~12 km-long and is running WSW–ENE along the southern flank of Elikon Mountain. The fault juxtaposes Mesozoic limestones and is characterized by steep, relatively undissected ridges and exposed fault surfaces along the top of a nearly continuous apron of scree, similar to faults elsewhere in Greece (i.e. Koukouvelas et al., 1999; Goldsworthy and Jackson, 2000). Polished surfaces cutting through cemented limestone breccias are occasionally exposed; they often contain corrugations with wavelengths of centimetres to meter documenting dip-slip kinematics. The surface trace of the fault is marked along much of its length by discrete 1–5 km-long fault segments.

The Leontari Fault is a ~13 km-long south facing normal fault located east of the Neochori Fault (Fig. 8a). The fault outcrops Neogene sediments forming an E–W trending low roughly linear hilly area (Goldsworthy and Jackson, 2000). Along its length a series of 1–7 km-long fault segments have been recognized in the digital topography, apparently controlling the drainage pattern and the landscape (Fig. 8a, b). The footwall topography of the Leontari Fault (~350 m a.s.l.) is overall subtler comparing with the Neochori Fault (~1000 m a.s.l.).

The mean mountain front sinuosities (S_{mf}) are 1.08 and 1.16 for the Neochori Fault and Leontari Fault respectively (see and Fig. 8c). Values of the measured segments for the Neochori Fault are the same (Fig. 8c), while for the Leontari Fault after a relative high value in its western part, the sinuosity progressively increases from 1.05 to 1.31, decreasing to a relatively lower value in its eastern part. The V_f mean value for the Neochori Fault is 0.46 increasing from west to east (Fig. 8e). The Leontari Fault has a mean V_f of 1.03 with a range of values from 0.13 to 3.85 and with a weak tendency for lower values to the east (Fig. 8e). Elongation ratios (drainage basin shape) for the Neochori Fault range from 1.35 to 2.57 (mean 2.11) and for the Leontari Fault from 1.16 to 4.27 (mean 2.19) (Fig. 8e). S_L values along the Neochori Fault (Fig. 8d) are high, indicating steeper relative slopes, near stream mouths, while S_L values along Leontari Fault are relatively low, probably associated with the soft sedimentary rocks affected by the fault.

The drainage network in the footwall of the two faults exhibits distinct differences. The footwall drainage network of the Neochori Fault is characterized by large catchments flowing almost perpendicular to the strike of the fault and oblique large catchments flowing around the fault tips (Fig. 8a). Two narrow gorges indicate deep incision of the uplifted footwall block at the central part of the Neochori Fault. The footwall drainage catchments of the Leontari Fault are smaller compared with those of the Neochori Fault. The Leontari footwall is characterized by a short in length, incised, system of sub-parallel streams flowing down the dip direction of the fault (Goldsworthy and Jackson, 2000). From west to east, the length of the footwall catchments decreases. In particular, the middle and western part of the Leontari Fault is marked by discreet groups of basins with progressive decreasing size to the east (Fig. 8a). Relatively larger catchments, in the west part of each group, may be related to their origin as major stream systems flowing around the relatively instantaneous fault tips and mark the

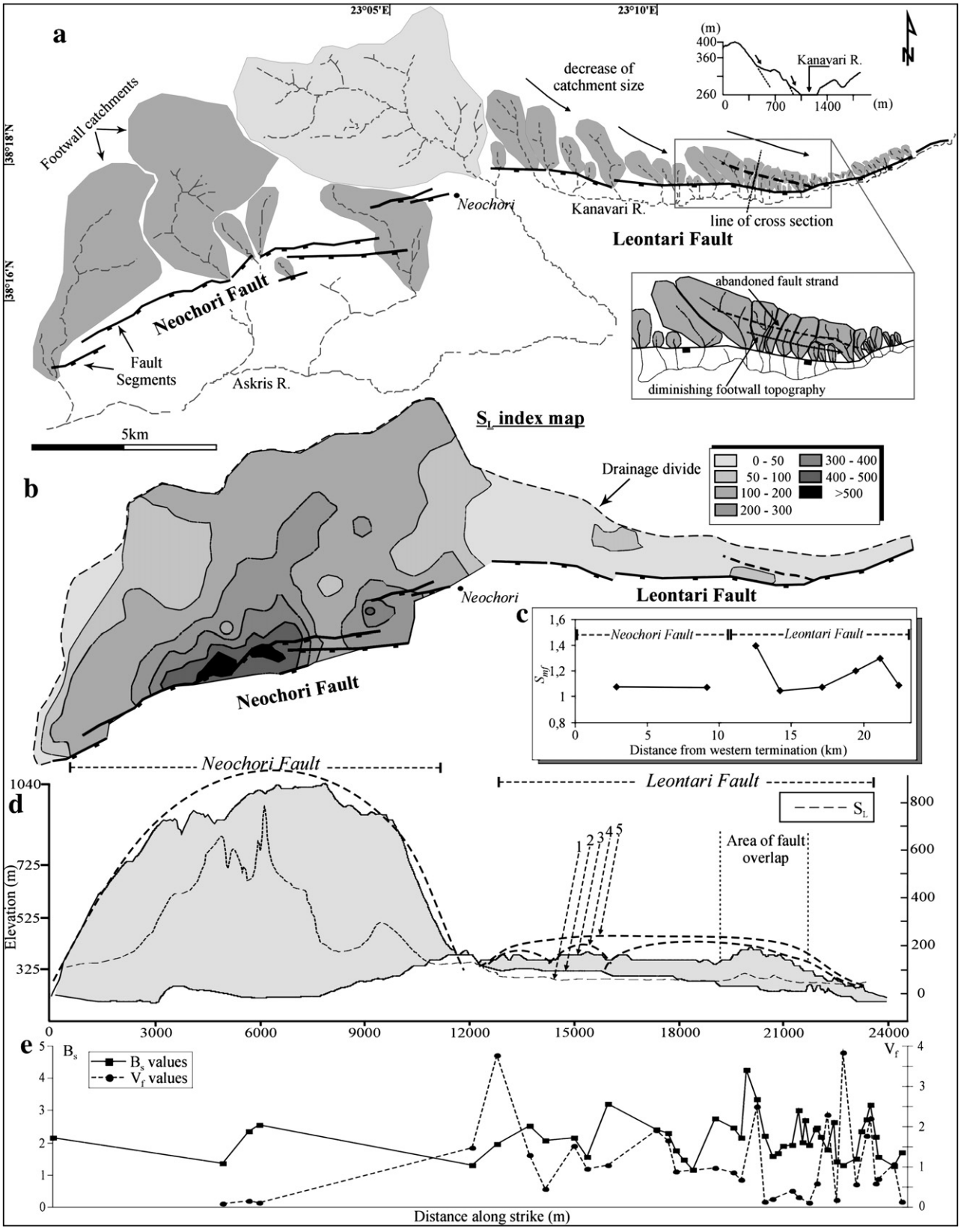

Fig. 8. The Neochori–Leontari Fault zone. (a) Footwall drainage catchments geometry and drainage network of the Neochori–Leontari faults. (b) Contour map of stream length-gradient index (S_L) values computed for all analyzed channels. (c) Mountain-front sinuosity (S_{mf}) along the fault scarps. (d) Large-scale displacement profile of the Neochori–Leontari Fault zone. Hanging-wall and footwall topographic profiles and S_L values are plotted versus distance along strike. 1: S_L values along strike; 2: Hanging-wall topographic profile; 3: Footwall topographic profile; 4: Smoothed topography of fault segments; 5: Overall smoothed fault topography. (e) Ratios of valley floor width to valley height (V_f) (dashed line) and basin elongation ratios (B_S) (solid line) along fault strike.

termination of the fault segments (Jackson and Leeder, 1994). In the central part and in the overlap zone of the two fault segments of the Leontari Fault, the streams have elongated catchments that flow perpendicular to their strike (Fig. 8a). The size of these catchments decreases to the point of the fault segment connection (Fig. 8a, inset). In this particular case a series of small catchments are incorporated in the footwall of the new propagating fault. Important for the fault propagation is also the complete absence of drainage at the easternmost tip of the fault. This combined with the complete parallelization of the Kanavari River and the low S_{mf} and V_f values suggest an eastward propagation of the fault.

The Askris and the Kanavari Rivers are axial drainage in the hanging-wall of the Neochori and Leontari Faults respectively. In the eastern part of the Leontari Fault the Kanavari River flows through the easternmost fault tip.

Fault segment boundaries are marked by local highs and lows in hanging-wall and footwall elevation profiles, respectively, and are commonly regarded as persistent barriers to fault rupture (Gawthorpe and Leeder, 2000; and references therein). The along-strike displacement profile of the Neochori Fault shows at its eastern tip a local high and low in hanging-wall and footwall topographic profiles, respectively (Fig. 8d). Although mapping along the Neochori range front suggests that the bounding fault is segmented, the footwall topography does not reveal significant slip deficits associated with the segment boundaries. The entire range can be treated as being controlled almost by a single fault. For the Leontari Fault, the generally smoothed footwall topography (line 5 in Fig. 8d) could be tentatively interpreted to consist of three minor segments (line 4 in Fig. 8d).

In summary, all geomorphic indices considered for the Neochori–Leontari fault zone show an active structure attaining a cumulative length of ~25 km. This fault zone consists of two prominent segments the Neochori and Leontari Faults, with the eastern segment of the fault zone likely still propagating eastward.

5.2. Livadostras–Kaparelli Fault zone

The Livadostras–Kaparelli Fault zone (Fig. 2), which is composed by the Livadostras and the Kaparelli Faults (Fig. 9) is located south of the Neochori–Leontari Fault zone.

The Livadostras Fault is responsible for a series of fault scarps running along the southern flank of Korompilli Mountain (Fig. 3 and cross-section BB′ in Fig. 4). Polished surfaces, cutting through cemented limestone breccias, are occasionally exposed along the fault, with a light-coloured ribbon at the base of the fault scarps. In the eastern part, the mapped fault segments form a left stepping fault zone. The westernmost fault segment is inferred to continue offshore within the Gulf of Corinth.

The Kaparelli Fault is an E–W trending south-dipping normal fault, which was ruptured during the third event (4th March) of the 1981 February–March earthquake swarm that affected the easternmost end of the Gulf of Corinth. The Kaparelli Fault is divided into two prominent fault segments the north and south Kaparelli Fault segments, spaced apart at about 3.5 km (Jackson et al., 1982; Papazachos et al., 1984a,b; Pavlides, 1993; Benedetti et al., 2003; Kokkalas and Koukouvelas, 2005). The length of the northern and southern fault segments is about 4.5 and 5 km, respectively. The north Kaparelli Fault segment lies on the southern side of a hill (~385 m a.s.l.), north of the Livadostras River. The footwall of this segment is composed of Mesozoic limestones, while the hanging-wall contains alluvial and colluvial deposits attaining a maximum thickness of c. 200 m (Tsodoulos and Koukouvelas, 2004; Kokkalas and Koukouvelas, 2005). The eastern termination of this segment turns abruptly to the southeast and crosses the alluvial deposits of the valley floor (Jackson et al., 1982; Pavlides, 1993). The western part of this segment is juxtaposing fluvial deposits of Pleistocene age (Jackson et al., 1982). The south Kaparelli Fault segment lies along the northwestern side of Kithaironas Mt. (Figs. 3 and 4). During the 1981 earthquake a series of discontinuous cracks with a NE–SW direction crossed the graben of the Livadostras River forming a step-over zone between the two segments (Jackson et al., 1982; Pavlides, 1993). The south Kaparelli Fault is at close proximity to the Kithairon Mt. and the drainage across the fault is absent.

The mean S_{mf} for the Livadostras and Kaparelli Fault is 1.13 and 1.14, respectively, decreasing eastwards for both fronts (Fig. 9c). The mean V_f value for Livadostras Fault is 0.30 and increases from west to east (Fig. 9e). The Kaparelli Fault has a mean V_f of 0.50 with a weak tendency for lower values to the east (Fig. 9e). Elongation ratios (Drainage basin shape) for the Livadostras Fault range from 1.43 to 8.38 (mean 3.11) and for Kaparelli Fault from 1.4 to 5.1 (mean 3.54) (Fig. 9e). The distribution of the values and the presence of a wind gap close to the eastern tip of the north Kaparelli Fault suggest an eastward propagation of the fault (Tsodoulos and Koukouvelas, 2004). S_L values along Livadostras Fault are high, indicating steeper relative slopes, near stream mouths, while S_L values along the Kaparelli Fault are relatively low (Fig. 9b). Exception to this pattern occurs in the area of fault overlap showing relatively high S_L values.

Drainage in the footwall of the faults is characterized by streams flowing perpendicular to the strike of the faults with deeply incised valleys. Relative large footwall catchments are observed along the fault, while some of the large catchments enter the graben at the tips of the fault segments.

The topography of the crest of the uplifted footwall for the Livadostras Fault reveals slip deficits (line 4 in Fig. 9d) associated with two main segment boundaries. The middle and east part of the fault although is segmented, this segmentation is not very well preserved on the footwall topography.

The general footwall topography (line 5 in Fig. 9d) of the north Kaparelli Fault is complex showing a complexly faulted limestone ridge and a topographic saddle (line 4 in Fig. 9d). However, the overall topography of the footwall is showing roughly a bell-shaped geometry suggesting the occurrence of segments and displacement deficits (lines 4 and 5 in Fig. 9d).

5.3. Erithres–Dafnes Fault zone

The Pastra Mountain range is in physical orographic continuity to the east of the Kithairon Mountain, with both of them cored by Mesozoic limestones and bounded on their northern flanks by two normal faults the Erithres and Dafnes Faults

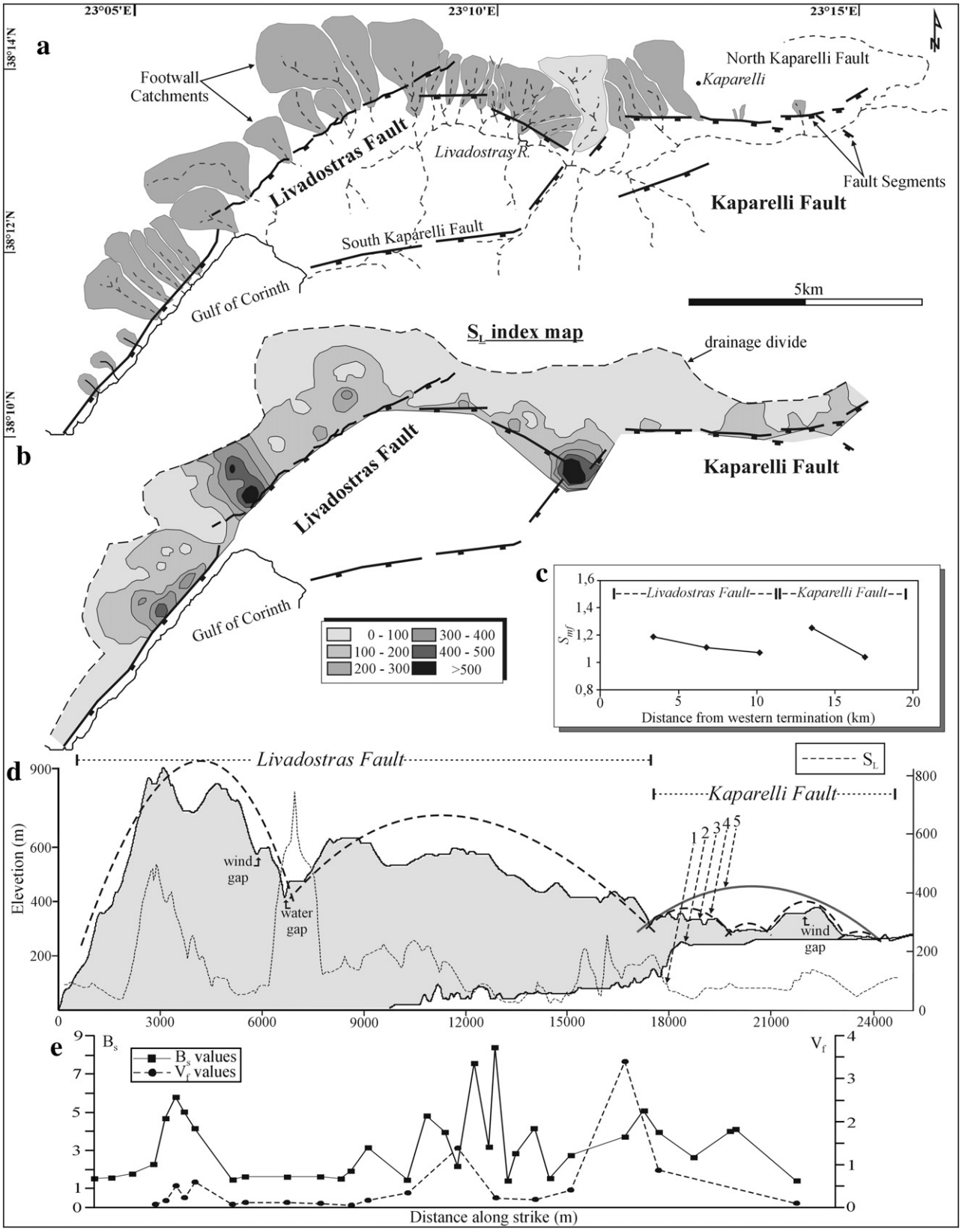

Fig. 9. The Livadostras–Kaparelli Fault zone. (a) Footwall drainage catchments geometry and drainage network of the Livadostras–Kaparell faults. (b) Contour map of stream length-gradient index (S_L) values computed for all analyzed channels. (c) Mountain-front sinuosity (S_{mf}) along the fault scarps. (d) Large-scale displacement profile of the Livadostras–Kaparelli Fault zone. Hanging-wall and footwall topographic profiles and S_L values graph versus distance along strike. 1: S_L values along strike; 2: Hanging-wall topographic profile; 3: Footwall topographic profile; 4: Smoothed topography of fault segments; 5: Overall smoothed fault topography. (e) Ratios of valley floor width to valley height (V_f) (dashed line) and basin elongation ratios (B_S) (solid line) along fault strike.

(Figs. 3 and 10). These two faults show a left-stepping overlap geometry configuration. Their overlap is ~2.5 km and have a spacing ~2 km (Fig. 10a).

The north facing Erithres Fault is a 12-km-long normal fault running along the northern flank of Kithairon Mountain in an almost E–W direction. Its trace is segmented in map view and the uplifted footwall of the fault reaches an elevation of ~1400 m.

The ENE–WSW trending Dafnes Fault is a northwest dipping normal fault along the north side of the Pastra Mountain, with a relief of ~1050 m. It is 15-km-long fault composed of eight discrete fault segments. The western part of the Dafnes Fault has a characteristic zigzag pattern, consisting of E–W and NE–SW-trending segments, while towards its eastern tip the NE–SW-trending segments are predominant (Fig. 10a).

The mean S_{mf} index is 1.25 and 1.26 for the Erithres Fault and Dafnes Fault, respectively (Fig. 10c). For the Erithres Fault only one front segment was calculated with a length of ~8 km (Fig. 10c), while for the Dafnes Fault the S_{mf} index was calculated for four range front segments. The western-half of the Dafnes Fault is characterized by low S_{mf} values, where physical linkage of the fault segments is predominant (Fig. 10b). Low S_{mf} values (~1.10) are also found at the eastern tip of the fault, where fault segments show a typical geometry of approaching segments. Exception to this is a relative high S_{mf} value (1.7), where the fault throw is low but the erosion is apparently high. Regarding the indices of drainage basin shape and V_f, (Fig. 10e), the Erithres Fault shows elongate basins with a B_s mean value of 3.12 (ranging from 1.62 to 4.78) and V-shaped stream valleys with low V_f values (0.49). Circular basins drained by streams showing high lateral erosion characterize the Dafnes Fault with mean B_s values of 2.21 (ranging from 1.33 to 6.24) and V_f values of 0.82. The distribution of the S_L index shows six spots of high S_L values (Fig. 10b). Maximum S_L values are concentrated where the fault changes its pattern from a zigzag geometry into a simple almost straight ENE-trending trace. The combination of the S_L index with the relief of the fault is not a simple task because S_L is calculated along streams, while S_L maxima concentrate where the relief is high. Only one exception is recognized at the easternmost tip where, though relief is reduced, all four streams show a high gradient feature that can be combined with low S_{mf} values. All these data, as well as the steepness of fault scarps in the area suggest that although the Dafnes Fault propagates at both tips, the easternmost tip of the fault propagates at a higher rate than the western tip.

Along the footwall of the Dafnes Fault, three large catchments behead one or more intervening basins. Following Jackson and Leeder (1994), a possible explanation for their large size is that the catchments incrementally expand toward and beyond the fault tips as the fault propagates. The size of these catchments relative to others suggests that their position along the fault was fixed for some time. If this model of footwall catchment evolution with respect to the fault propagation is correct then large footwall catchments highlight the old fault tips. This implies that the Dafnes Fault might have grown episodically and that periods of quiescence are suggested by the large drainage systems established at the fault tips. In addition, the eastern tips of the fault show a strong impact on the drainage pattern with high S_L values, V-shaped valleys and elongate basins, which is of interest for the propagation of the fault zone.

As faults grow and their tips overlap, one fault may predominate over the other and accommodate some of the displacement which was previously taken up on the other fault (Jackson and Leeder, 1994; Burbank and Anderson, 2001). The drainage in the overlap of the Erithres and Dafnes Faults is characterized by small, elongate drainage basins that flow perpendicular to strike. Streams immediately west of the Dafnes Fault are incised in the hanging-wall of the Erithres Fault, up to a distance of ~1 km west of the mapped fault termination. Weir to the enfluded streams and adjacent to the Erithres Fault the streams are not incised except locally at their heads. In addition, the decease of the topographic relief along the footwall of the Dafnes Fault (Fig. 10a) suggests that the Dafnes Fault propagates westward accumulating displacement at the expense of the Erithres Fault, which propagates to the east as it is denoted by wind-gaps and a water-gap.

The two easternmost fault segments of the Dafnes Fault exhibit a quite similar situation, as described for the Dafnes–Erithres overlap zone, with river deflection into the area between the fault tips and entrenchment of the stream along the front fault segment.

The Asopos River is an axial drainage in the hanging-wall of the Dafnes Fault. After flowing through the Pliocene deposits of the Thiva basin, the river is then deflected and incised in the hanging-wall of the Dafnes Fault near the easternmost tip of the fault.

The topography of the crest of the uplifted footwall of the Dafnes Fault reveals slip deficits (dashed lines) associated with the segment boundaries (Fig. 10d). Although the western part of the fault is segmented, the footwall topography does not show any significant slip deficit associated with segment boundaries. Accordingly, the west part of the Dafnes Range can be considered, as controlled by a single fault. The general footwall topography of the Dafnes Fault (line 5 in Fig. 10d) shows asymmetry to the west, where the two major bounding faults interact. The topography of the hanging-wall is complicated and even though some intrabasin highs are recognized within the hanging-wall of the fault, their relationship with the boundaries of the fault segments is not very clear. Bell-shaped footwall topography of the Erithres Fault suggests the occurrence of two segments (line 4 in Fig. 10d). Each of these two interpreted segments corresponds to more than one mapped fault segments, but they do not represent displacement deficits in the footwall topography. Intrabasinal highs are recognized in the hanging-wall topography of the Erithres Fault that corresponds to segments boundaries.

In summary, all indices considered for the Erithres–Dafnes fault zone show an active structure attaining a length of ~27 km. This structure is separated into two prominent segments with the eastern segment showing higher tectonic activity.

5.4. Kallithea–Asopia Fault zone

The Kallithea–Asopia Fault zone defines a WNW-trending 6-km-wide intrabasin high in the Thiva Basin defined by a

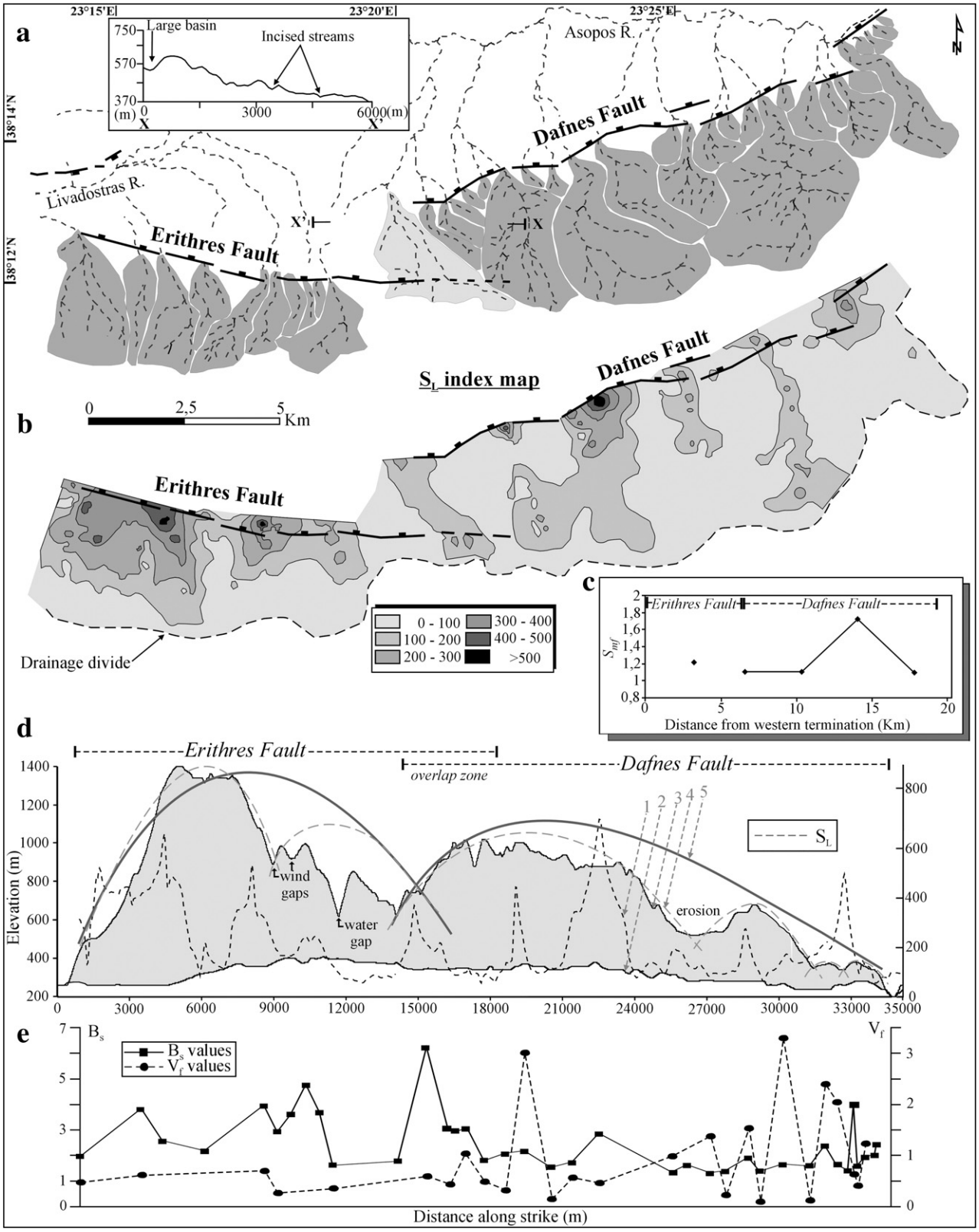

Fig. 10. The Erithres–Dafnes Fault zone. (a) Footwall drainage catchments geometry and drainage network of the Erithres–Dafnes faults. (b) Contour map of stream length-gradient index (S_L) values computed for all analyzed channels. (c) Mountain-front sinuosity (S_{mf}) along the fault scarps. (d) Large-scale displacement profile of the Erithres–Dafnes Fault zone. Hanging-wall and footwall topographic profiles and S_L values graph versus distance along strike. 1: S_L values along strike; 2: Hanging-wall topographic profile; 3: Footwall topographic profile; 4: Smoothed topography of fault segments; 5: Overall smoothed fault topography. (e) Ratios of valley floor width to valley height (V_f) (dashed line) and basin elongation ratios (B_S) (solid line) along fault strike.

system of extensional faults (Fig. 2). In map view, these faults generate a ~18 km-long range of Mesozoic limestones (Fig. 3). All mapped faults of the Kallithea–Asopia Fault zone trend WNW–ESE showing divergent settings (Fig. 11).

The mapped faults in the Kallithea–Asopia Fault zone are all segmented in plan view: i.e. they are composed of a number of discrete minor segments (Fig. 11). The segment boundaries of the Kallithea–Asopia Fault zone are commonly characterized by relay structures (Tsodoulos and Koukouvelas, 2005; Sboras, 2007) that exhibit a range of structural styles that are broadly comparable with the evolutionary scheme of relay-ramp geometry proposed by Peacock and Sanderson (1991). According to this evolutionary scheme, relay structures proceed from a stage where fault segments overlap with an intervening relay-ramp, to a more evolved stage where the relay-ramp is broken down by internal faulting and a through-going fault zone connects the overlapping segments (Figs. 11 and 12). All bounding normal faults in the Kallithea–Asopia Fault zone expose polished surfaces that are cutting through cemented limestone breccias. They often contain corrugations, with wavelengths of centimetre to meters, documenting an almost pure dip-slip kinematics. Light-coloured ribbons at the base of the fault scarps probably suggest recent activity of the fault during past linear morphogenic earthquakes sensu (Caputo, 2005).

The footwall drainage in the Kallithea–Asopia Fault zone is affected by secondary faulting (Fig. 11). The eastern part of the fault zone exhibits relative large footwall drainage basins (Fig. 11) with low elongation ratio (Fig. 12). The drainage enters the basin at the tips of fault segments or between echelon steps. The drainage from the steep fault surfaces is minor or is missing. The footwall drainage of the bounding faults at the western part of the fault zone is characterized by relative small and elongated footwall catchments flowing perpendicular to the fault strike and relatively large catchments are placed at the western tips of the faults. Large basins inward of the present-day tips of the faults suggest propagating faults. Small basins with low elongation ratio characterize the eastern tips of the faults. Axial streams flowing along the strike of the fault segments characterize the drainage in the hanging-wall of the main bounded faults.

The values of the V_f index for the studied fronts of the Kallithea–Asopia Fault zone ranges from about 0.58 (Kirikion Fault) to 1.64 (Asopia Fault), while B_s values range from 1.87 to 2.4. The mountain front sinuosity (S_{mf}) for this area is very low (~1.10) for all the studied fronts.

The studied range fronts of the Kallithea–Asopia Fault zone have been interpreted as being bounded by segmented normal faults for most of which there is some correspondence between the segment boundaries and the topographic lows in the footwall. Topographic profiles of the crest of the uplifted footwalls for the Kallithea–Asopia Fault zone reveal slip deficits (line 3 Fig. 12) associated with the segment boundaries.

6. Discussion

Drainage patterns and geomorphology at topographic fronts typically shed light on how the faults grow or if these faults show relatively “high” or “low” tectonic activity. In specific cases, geomorphic parameters calculated at topographic fronts can also be used for evaluating if a fault is more active with respect to other faults. In addition, the surface change attributable to past seismic events typically extends considerably beyond the fault

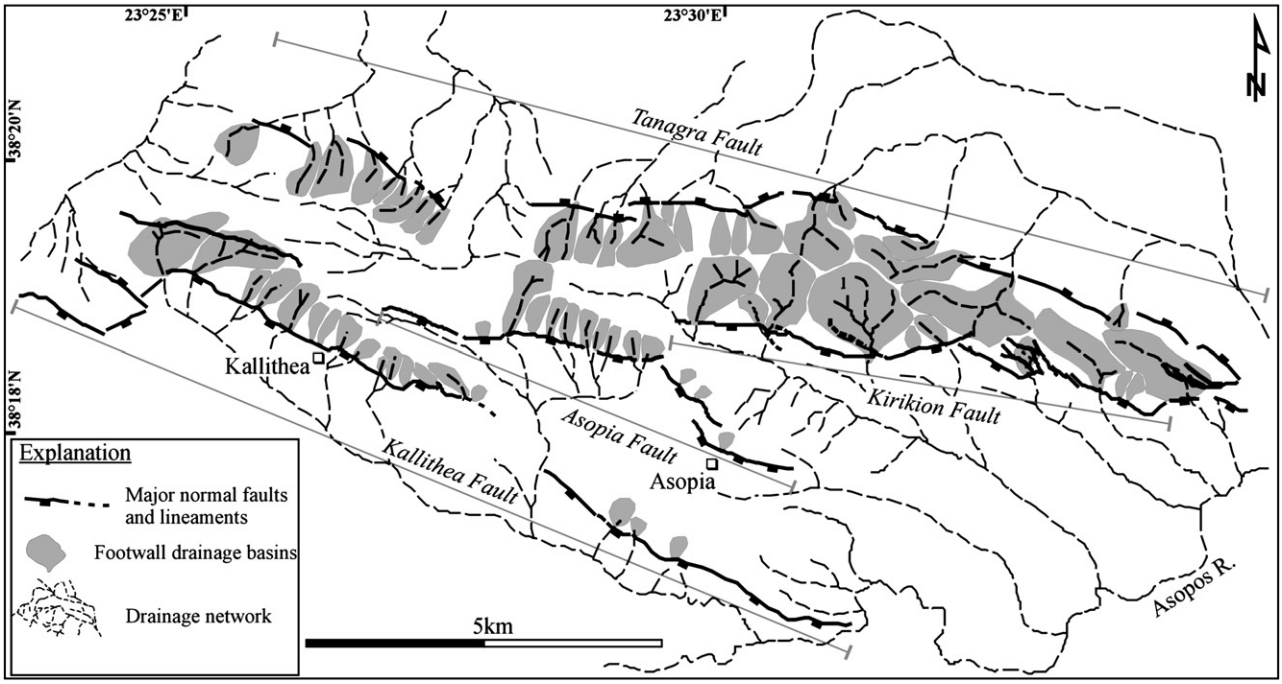

Fig. 11. Detailed fault map with footwall drainage catchments geometry and drainage network of the Kallithea–Asopia Fault Zone.

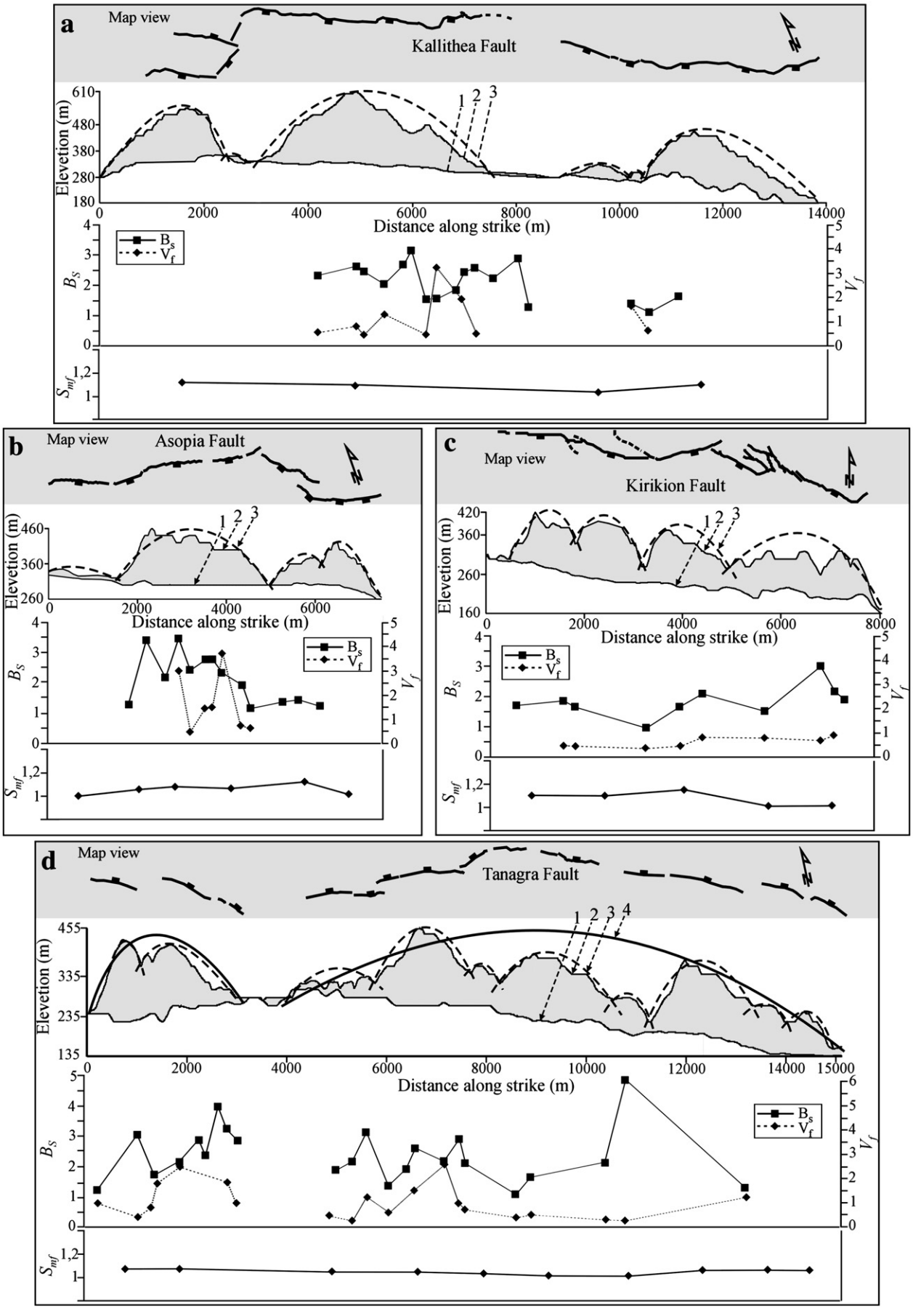
a
Map view
Kallithea Fault
Elevetion (m)
610
480
380
280
180
1 2 3
0 2000 4000 6000 8000 10000 12000 14000
Distance along strike (m)
B_s
V_f
B_S
V_f
S_mf
1,2
1
b
Map view
Asopia Fault
Elevetion (m)
460
360
260
1 2 3
0 2000 4000 6000
Distance along strike (m)
B_s
V_f
B_S
V_f
S_mf
1,2
1
c
Map view
Kirikion Fault
Elevetion (m)
420
360
260
160
1 2 3
0 2000 4000 6000 8000
Distance along strike (m)
B_s
V_f
B_S
V_f
S_mf
1,2
1
d
Map view
Tanagra Fault
Elevetion (m)
455
335
235
135
1 2 3 4
0 2000 4000 6000 8000 10000 12000 14000 15000
Distance along strike (m)
B_s
V_f
B_S
V_f
S_mf
1,2
1

itself. Even when deformation is rather tightly limited to the fault zone, the geomorphic response to the deformation can propagate away from the fault zone to affect other parts of the landscape (Burbank and Anderson, 2001). It is suggested that a series of parameters change after strong events (Keller and Pinter, 2002). Therefore, in an area like the Aegean the study of landscape by means of geomorphic parameters can shed light to the impact of earthquakes on the landscape.

Understanding the tectonic evolution of the study area is important, because of its position between two major fault systems, the Gulf of Corinth and the Northern Gulf of Evia. All faults or fault zones analyzed in this study control a basin and range topography accommodating the current extension in the South Sterea Hellas region. These faults follow two trends: ENE to NE and WNW to E–W (Figs. 1 and 2). The former fault system prevails in western Greece, with Rio Graben as a typical structure controlled by these faults (Fig. 1) (Kokkalas et al., 2006). In eastern Peloponnese and south Sterea Hellas this fault system appears to be weaker (Koukouvelas et al., 1996; Doutsos and Kokkalas, 2001). The Livadostras, Neochori and Dafnes faults belong to this fault trend. The WNW to E–W trending faults control a series of typical grabens, like the Gulf of Corinth, Tithorea, Sperchios–Atalanti as well as the Thiva graben (Doutsos and Piper, 1990; Roberts and Koukouvelas, 1996; Doutsos and Kokkalas, 2001; Goldsworthy et al., 2002; Ganas et al., 2005). The Kaparelli, Leontari, Tanagra, Kallithea, Asopia, Kirikion and Erithres faults belong to this fault trend. All mentioned faults are organized in fault zones. It is also commonly observed that faults belonging to the two fault trends show a physical or mechanical linkage and thus in the same fault zone both fault trends are included. Based on this remark we combine all analyzed faults in four large fault zones (Figs. 8–12).

Displacement profiles used as estimates of minimum vertical displacements suggest that total displacement along the ENE to NE-trending faults are generally larger than displacements along the WNW to E–W trending faults. An exception is represented by the Erithres Fault that shows high displacement (Fig. 10). Although it is beyond the scope of this study to explain why NE-trending faults are characterized by larger displacements, we suggest that this seems to be related to the age of the faults with the first trend to be older than the second (see also Kokkalas et al., 2006 and references therein). Regarding the other geomorphic analyzed parameters, all faults display V_f values ranging between 0.5 and 1.6, the S_{mf} values range from 1.08 to 1.26, while the B_s values range from 1.8 to 3.54. These values show that all analyzed fault zones are active (sensu Bull and McFadden, 1977; Ramirez-Herrera, 1998; Keller and Pinter, 2002; Salvany, 2004). Regarding the S_L index, high values were estimated close to the fault trace, further documenting the notion that all fault zones are active. The evaluation of S_L over the study area suggests that all the fronts, which are defined by the four fault zones, yield high rates of uplift (Fig. 7). Finally, regarding the Transverse Topographic Symmetry Factor and the Asymmetry Factor both suggest a predominant tilting of the basin floor towards WNW-trending faults. In one case, the Askris River shows, tilting related to the NE-trending Neochori fault (Fig. 6).

Geomorphic criteria useful in evaluating rates and direction of lateral propagation of active folds in the direction of lateral propagation have been proposed (Keller et al., 1999; Keller and Pinter, 2002). Although these criteria were derived for the identification of fault propagation of reverse faults by Keller and Pinter (2002), the normal faults in the Thiva Basin seem to follow a similar pattern and the use of the geomorphic criteria appears to be appropriate. The geomorphic criteria for the identification of the direction of normal fault propagation along the fault zones that are used includes towards their tips areas the following: (1) decrease in topographic relief, (2) decrease in relief of water and wind-gaps, (3) diverted drainage at the propagating fault tip, (4) deformation of younger deposits. In the Thiva Basin, the following characteristics are documented along the four fault zones: (a) footwall relief decreases and relief of water and wind-gaps decrease to the east, (b) all diverted drainage and alignment of rivers are prominent at the eastern fault tips, while along the western tip areas the drainage crosses the tip areas at high angles, and finally (c) progressive deformation of younger sediments is concentrated at the east tip of the faults.

7. Conclusions

1) The analysis of one geomorphic parameter typically exhibits limitations or even contradicting results due to lithological differentiations or the location of the fault within the studied basin. Our analysis is based on the application of more than one parameter in the study area and leads to more meaningful results than of those a single parameter analysis would provide.
2) Fault zones in the study area range in length from 10–30 km. Although these zones define a more or less continuous range, the geomorphic parameters show that segmentation of faults is the dominant geometry for normal faults within the eastern-most sector of the Gulf of Corinth. Major segments are in the order of 10 km in length and resemble more or less the length of co-seismic surface rupture during the past morphogenic earthquakes in the Gulf of Corinth or in central Greece.
3) Tectonic geomorphology analysis of the four studied fault zones suggests that all of them are characterized as highly active.
4) Although fault zones controlling the Thiva Basin show lateral growth both westwards and eastwards, in several cases the tendency for eastward lateral growth is more predominant.
5) The basin asymmetry analysis, based on the *T* and AF factors, allows interpretation of their asymmetry due to active faulting and apparently indicates that all studied basins show tilting, mainly controlled by the WNW to E–W trending normal faults.

Fig. 12. Large-scale displacement profiles and plots of ratios of valley floor width to valley height (V_f), basin elongation ratios (B_S) and Mountain-front sinuosity (S_{mf}) along fault strike for the Kallithea Fault (a), the Asopia Fault (b), the Kirikion Fault (c) and the Tanagra Fault (d). 1: Hanging-wall topographic profile; 2: Footwall topographic profile; 3: Smoothed topography of fault segments; 4: Overall smoothed fault topography.

Acknowledgements

At the time of research, IT was funded by the Greek State Scholarship's Foundation (I.K.Υ.). SP and IK were supported by OASP (Earthquake Planning and Protection Organization of Greece- Project 27/53874/20-11-00) and program B095 (Karatheodoris) respectively. We would like to thank E.A Keller, B. Pace and S. Kokkalas for constructive criticism and R. Caputo for the editorial support.

References

Ambraseys, N.N., Jackson, J.A., 1990. Seismicity and associated strain of central Greece between 1890 and 1988. Geophysical Journal International 101, 663–708.

Ambraseys, N.N., Jackson, J.A., 1997. Seismicity and strain in the Gulf of Corinth (Greece) since 1694. Journal of Earthquake Engineering 1 (3), 433–474.

Ambraseys, N.N., Jackson, J.A., 1998. Faulting associated with historical and recent earthquakes in the Eastern Mediterranean region. Geophysical Journal International 133, 390–406.

Angelier, J., Lyberis, N., Le Pichon, X., Barrier, E., Huchon, P., 1982. The tectonic development of the Hellenic Arc and the Sea of Crete. Tectonophysics 86, 159–196.

Azor, A., Keller, E.A., Yeats, R.S., 2002. Geomorphic indicators of active fold growth: South Mountain-Oak Ridge anticline, Ventura basin, southern California. Geological Society of American Bulletin 114, 745–753.

Barry, R.G., Chorley, R.J., 1998. Atmosphere, Weather and Climate, 7th Edition. Routledge, New York.

Benedetti, L., Finkel, R., King, G., Armijo, R., Papanastassiou, D., Ryerson, F.J., Flerit, F., Farber, D., Stravrakakis, G., 2003. Motion on the Kaparelli fault (Greece) prior to the 1981 earthquake sequence determined from ^{36}Cl cosmogenic dating. Terra Nova 15, 118–124. doi:10.1046/j.1365-3121.2003.00474.x.

Billiris, H., Paradissis, D., Veis, G., England, P., Featherstone, W., Parsons, B., Cross, P., Rayson, M., Sellers, P., Askenasi, V., Davison, M., Jackson, J.A., Ambraseys, N., 1991. Geodetic determination of tectonic deformation in central Greece from 1900 to 1988. Nature 350, 124–129.

Boronkay, K., Doutsos, T., 1994. Transpression and transtension within different structural levels in the central Aegean region. Journal of Structural Geology 16, 1555–1573.

Briole, P., Rigo, A., Lyon-Caen, H., Ruegg, J.C., Papazissi, K., Mitsakaki, C., Balodimou, A., Veis, G., Hatzfield, D., Deschamps, A., 2000. Active deformation of the Corinth rift, Greece: results from repeated Global Positioning System surveys between 1990 and 1995. Journal of Geophysical Research 105, 25,605–25,625. doi:10.1029/2000JB900148.

Bull, W.B., McFadden, L.D., 1977. Tectonic geomorphology north and south of the Garlock fault, California. In: Doehring, D.O. (Ed.), Proceedings of Eighth Annual Geomorphology Symposium, Geomorphology in Arid Regions. State University of New York, Binghamton, pp. 115–138.

Burbank, D.W., Anderson, R.S., 2001. Tectonic Geomorphology. Blackwell Science, Massachusetts.

Burbank, D.W., Pinter, N., 1999. Landscape evolution: the interactions of tectonics and surface processes. Basin Research 11, 1–6.

Caputo, R., 2005. Ground effects of large morphogenic earthquakes. Journal of Geodynamics 40 (2–3), 113–118.

Caputo, R., Pavlides, S., 1993. Late Cainozoic geodynamic evolution of Thessaly and surrounding (Central-Northern Greece). Tectonophysics 223, 339–362.

Cartwright, J.A., Trudgill, B.D., Mansfield, C.S., 1995. Fault growth by segment linkage: an explanation for scatter in maximum displacement and trace length data from the Canyonlands grabens of SE Utah. Journal of Structural Geology 17, 1319–1326.

Christodoulou, G.E., 1969. On the geology of the Thivai–Paralimni area. Geological and geophysical research. Institute for Geology and Subsurface Research, Athens 13 (1).

Clarke, P.J., Davies, R.R., England, D.C., Parsons, B., Billiris, H., Paradissis, D., Veis, G., Cross, P.A., Denys, P.H., Ashkenazi, V., Bingley, R., Kahle, H.-G., Muller, M.V., Briole, P., 1998. Crustal strain in central Greece from repeated G.P.S., measurements in the interval 1988–1997. Geophysical Journal International 135, 195–214.

Collier, R.E.L., Leeder, M.R., Jackson, J.A., 1995. Quaternary drainage development, sediment fluxes and extensional tectonics in Greece. In: Lewin, J., Macklin, M.G., Woodward, J.C. (Eds.), Mediterranean Quaternary River Environments. Publ. A.A. Balkema, Rotterdam, pp. 31–44.

Cox, R.T., 1994. Analysis of drainage-basin symmetry as a rapid technique to identify areas of possible Quaternary tilt-block tectonics: an example from the Mississippi Embayment. Geological Society of America Bulletin 106, 571–581. doi:10.1130/0016- 7606(1994)106<0571:AODBSA>2.3.CO;2.

Cox, R.T., Van Arsdale, R.B., Harris, J.B., 2001. Identification of possible Quaternary deformation in the northeastern Mississippi Embayment using quantitative geomorphic analysis of drainage-basin asymmetry. Geological Society of America Bulletin 113 (5), 615–624. doi:10.1130/0016-7606(2001)113<0615: IOPQDI>2.0.CO;2.

Curray, J.R., 1956. Analysis of two-dimensional orientation data. Journal of Geology 64 (2), 117–131.

Davies, R.R., England, P.C., Parsons, B.E., Billiris, H., Paradissis, D., Veis, G., 1997. Geodetic strain of Greece in the interval 1892–1992. Journal of Geophysical Research 102 (B11), 24 571–24 588.

Davis, J.C., 2002. Statistics and Data Analysis in Geology. Wiley and Sons, New York.

Dawers, N.H., Anders, M.H., 1995. Displacement-length scaling and fault linkage. Journal of Structural Geology 17 (5), 607–614.

Degnan, P.J., Robertson, A.H.F., 1998. Mesozoic–early Tertiary passive margin evolution of the Pindos ocean (NW Peloponnese, Greece). Sedimentary Geology 117, 33–70. doi:10.1016/S0037-0738(97)00113-9.

Dounas, A., 1971. The Geology of the area between Megara and Erythrai village (Attica). Geological and geophysical Research, IGME, Publ. No 2, t. 15, Athens.

Doutsos, T., Piper, D.J.W., 1990. Listric faulting, sedimentation, and morphological evolution of the Quaternary eastern Corinth rift, Greece: first stages of continental rifting. Geological Society of American Bulletin 102, 812–829.

Doutsos, T., Kokkalas, S., 2001. Stress and deformation patterns in the Aegean region. Journal of Structural Geology 23, 455–472.

Doutsos, T., Koukouvelas, I.K., Xypolias, P., 2006. A new orogenic model for the External Hellenides. In: Robertson, A.H.F., Mountrakis, D. (Eds.), Tectonic Development of the Eastern Mediterranean Region. Special Publications, vol. 260. Geological Society of London, pp. 507–520.

Doutsos, T., Koukouvelas, I., Zelilidis, A., Kontopoulos, N., 1994. Intracontinental wedging and post-orogenic collapse in the Mesohellenic Trough. Geologische Rundschau 83, 257–275.

Eliet, P.P., Gawthorpe, R.L., 1995. Drainage development and sediment supply within rifts, examples from the Sperchios basin, central Greece. Journal of the Geological Society of London 152, 883–893.

Ganas, A., Pavlides, S., Karastathis, V., 2005. DEM-based morphometry of range-front escarpments in Attica, central Greece, and its relation to fault slip rates. Geomorphology 65, 301–319.

Ganas, A., Pavlides, S.B., Sboras, S., Valkaniotis, S., Papaioannou, S., Alexandris, G.A., Plessa, A., Papadopoulos, G.A., 2004. Active fault geometry and kinematics in Parnitha Mountain, Attica, Greece. Journal of Structural Geology 26, 2103–2118. doi:10.1016/j.jsg.2004.02.015.

Garrote, J., Cox, R.T., Swann, C., Ellis, M., 2006. Tectonic geomorphology of the southeastern Mississippi Embayment in northern Mississippi, USA. Geological Society of America Bulletin 118 (9/10), 1160–1170. doi:10.1130/B25721.1.

Gawthorpe, R.L., Hurst, J.M., 1993. Transfer zones in extensional basins: their structural style and influence on drainage development and stratigraphy. Journal of the Geological Society of London 150, 1137–1152.

Gawthorpe, R.L., Leeder, M.R., 2000. Tectono-sedimentary evolution of active extensional basins. Basin Research 12, 195–218.

Goldsworthy, M., Jackson, J.A., 2000. Active normal fault evolution in Greece revealed by geomorphology and drainage patterns. Journal of Geological Society of London 157, 967–981.

Goldsworthy, M., Jackson, J.A., Haines, J., 2002. The continuity of active fault systems in Greece. Geophysical Journal International 148, 596–618.

Griffiths, S.J., Street-Perrot, A., Holmes, J.A., Leng, M.J., Tzedakis, P.C., 2002. Chemical and isotopic composition of modern water bodies in the Lake Kopais Basin, central Greece. Sedimentary Geology 148, 79–103.

Hack, J., 1973. Stream profile analysis and stream gradient index. U.S. Geological Survey Journal Research Exploration, Athens 1, 421–429.

Hare, P.H., Gardner, T.W., 1985. Geomorphic indicators of vertical neotectonism along converging plate margins, Nicoya Peninsula, Costa Rica. In: Morisawa, M., Hack, J.T. (Eds.), Tectonic Geomorphology. Allen and Unwin, Boston, pp. 75–104.

Hatzfeld, D., Karakostas, V., Ziazia, M., Kassaras, I., Papadimitriou, E., Makropoulos, K., Voulgaris, N., Papaioannou, C., 2000. Microseismicity and faulting geometry in the Gulf of Corinth (Greece). Geophysical Journal International 141, 438–456.

Hilton, K., 1979. Progress and Pattern in Physical Geography. University Tutorial Press Limited, London.

Jackson, J.A., 1994. Active tectonics of the Aegean region. Annual Review of Earth and Planetary Sciences 22, 239–271. doi:10.1146/annurev.ea.22.050194.001323.

Jackson, J.A., 1999. Fault death: a perspective from actively deforming regions. Journal of Structural Geology 21, 1003–1010.

Jackson, J.A., Leeder, M., 1994. Drainage systems and the development of normal faults: an example from Pleasant Valley, Nevada. Journal of Structural Geology 16, 1041–1059.

Jackson, J.A., Gagnepain, J., Houseman, G., King, G.C.P., Papadimitriou, P., Soufleris, C., Virieux, J., 1982. Seismicity, normal faulting, and the geomorphological development of the Gulf of Corinth (Greece): the Corinth earthquakes of February and March 1981. Earth and Planetary Science Letters 57, 377–397. doi:10.1016/0012-821X(82)90158-3.

Keller, E.A., 1986. Investigation of active tectonics: use of surficial earth processes. In: Wallace, R.E. (Ed.), Active Tectonics, Studies in Geophysics. National Academy Press, Washington, DC, pp. 136–147.

Keller, E.A., Pinter, N., 2002. Active Tectonics: Earthquakes, Uplift and Landscape. Prentice Hall, New Jersey.

Keller, E.A., Gurrola, L., Tierney, T.E., 1999. Geomorphic criteria to determine direction of lateral propagation of reverse faulting and folding. Geology 27, 515–518.

King, G.C.P., Ouyang, Z.X., Papadimitriou, P., Deschamps, A., Gagnepain, J., Houseman, G., Jackson, J.A., Soufleris, C., Virieux, J., 1985. The evolution of the Gulf of Corinth (Greece): an aftershock study of the 1981 earthquakes. Geophysical Journal of the Royal Astronomical Society 80, 677–693.

Kokkalas, S., Koukouvelas, I., 2005. Fault-scarp degradation modeling in central Greece: the Kaparelli and Eliki faults (Gulf of Corinth) as a case study. Journal of Geodynamics 40 (2–3), 200–215 Special Issue.

Kokkalas, S., Xypolias, P., Koukouvelas, I., Doutsos, T., 2006. Postcollisional contractional and extensional deformation in the Aegean region. In: Dilek, Y., Pavlides, S. (Eds.), Postcollisional Tectonics and Magmatism in the Mediterranean region and Asia. Geological Society of America, Special Paper, vol. 409, pp. 97–123. doi:10.1130/2006.2409(06).

Koukouvelas, I., 1998. The Egion Fault: earthquake related and long term deformation, Gulf of Corinth, Greece. Journal of Geodynamics 26 (2–4), 501–513.

Koukouvelas, I.K., Doutsos, T., 1996. Implications of structural segmentation during earthquakes: the 1995 Egion earthquake, Gulf of Corinth, Greece. Journal of Structural Geology 18 (12), 1381–1388. doi:10.1016/S0191-8141(96)00071-5.

Koukouvelas, I.K., Asimakopoulos, M., Doutsos, T., 1999. Fractal characteristics of active normal faults: an example of the eastern Gulf of Corinth, Greece. Tectonophysics 308, 263–274. doi:10.1016/S0040-1951(99) 00087-6.

Koukouvelas, I., Mpresiakas, A., Sokos, E., Doutsos, T., 1996. The tectonic setting and earthquake ground hazards of the 1993 Pyrgos earthquake, Peloponnese, Greece. Journal of the Geological Society of London 153, 39–49.

Koukouvelas, I., Stamatopoulos, L., Katsonopoulou, D., Pavlides, S., 2001. A palaeoseismological and geoarchaeological investigation of the Eliki fault, Gulf of Corinth, Greece. Journal of Structural Geology 23, 531–543. doi:10.1016/S0191-8141(00)00124-3.

Le Pichon, X., Angelier, J., 1979. The Hellenic Arc and Trench system: a key to the Neotectonic evolution of the eastern Mediterranean area. Tectonophysics 60, 1–42.

Leeder, M.R., McNeill, L.C., Collier, R.E.L., Portman, C., Rowe, P.J., Andrews, J.E., Gawthorpe, R.L., 2003. Corinth rift margin uplift: new evidence from Late Quaternary marine shorelines. Geophysical Research Letters 30, 1611–1614.

Leeder, M.R., Seger, M., Stark, C.P., 1991. Sedimentology and tectonic geomorphology adjacent to active and inactive normal faults in the Megara basin and Alkyonides Gulf, Central Greece. Journal of the Geological Society of London 148, 331–343.

Mayer, L., 1986. Tectonic geomorphology of escarpments and mountain fronts. In: Wallace, R.E. (Ed.), Active Tectonics, Studies in Geophysics. National Academy Press, Washington, DC, pp. 125–135.

Mayer, L., 2000. Application of digital elevation models to macroscale tectonic geomorphology. In: Summerfield, M.A. (Ed.), Geomorphology and Global Tectonics. John Wiley & Sons Ltd, pp. 15–27.

McKenzie, D.P., 1972. Active tectonics of the Mediterranean region. Geophysical journal of the Royal Astronomical Society 30 (2), 109–185.

McKenzie, D.P., 1978. Active tectonics of the Alpine–Himalayan belt: the Aegean Sea and surrounding regions. Geophysical journal of the Royal Astronomical Society 55, 217–254.

Mercier, J.L., Delibassis, N.D., Gauthier, A., Jarrige, J.J., Lemeille, F., Philip, H., Sebrier, M., Sorel, D., 1979. La Neotectonique de l'Arc Egeen. Revue de Géologie Dynamique et de géographie Physique 67–92 Spec. Publ. No. 21.

Mettos, A., Ioakim, C., Rondoyanni, T., 2000. Palaeoclimatic and palaeogeographic evolution of Attica–Beotia (central Greece). Geological Society of Greece 9, 187–196 Special Publication.

Micarelli, L., Moretti, I., Daniel, J.M., 2003. Structural properties of rift related normal faults: the case study of the Gulf of Corinth, Greece. Journal of Geodynamics 36, 275–303. doi:10.1016/S0264-3707(03) 00051-6.

Okuda, M., Yasuda, Y., Setoguchi, T., 2001. Middle to Late Pleistocene vegetation history and climatic changes at Lake Kopais, Southeast Greece. Boreas 30, 73–82.

Onorati, G., Poscolieri, M., Ventura, R., Chiarini, V., Crucilla, U., 1992. The digital elevation model of Italy for geomorphology and structural geology. Catena 19, 147–178.

Papadopoulos, G., Vassilopoulou, A., Plessa, A., 2000. A new catalogue of historical earthquakes in the Corinth rift Central Greece: 480 BC–AD 1910. In: Papadopoulos, G. (Ed.), Historical Earthquakes and Tsunamis in the Corinth rift, Central Greece. National Observatory of Athens, Institute of Geodynamics, Publication No. 12, 9–119. National Observatory of Athens, Athens.

Papazachos, B., Papazachou, C., 1997. The Earthquakes of Greece. Editions ZITI, Thessaloniki, Greece.

Papazachos, B., Comninakis, P., Papadimitriou, E., Scordilis, E., 1984a. Properties of the February–March 1981 seismic sequence in the Alkyonides gulf of central Greece. Annales Geophysicae 5, 537–544.

Papazachos, B.C., Kiratzi, A., Hatzidimitriou, P., Rocca, A., 1984b. Seismic faults in the Aegean area. Tectonophysics 106, 71–85.

Paraskevaidis, I., 1971. Development of Viotika lakes Iliki and Paralimni. Bulletin Central Constructions, Athens 3–4, 3–14.

Pavlides, S., 1993. Active faulting in multi-fractured seismogenic areas: examples from Greece. Zeitschrift für Geomorphologie N.F. 94, 57–72.

Pavlides, S.B., Koukouvelas, I.K., Kokkalas, S., Stamatopoulos, L., Keramydas, D., Tsodoulos, I., 2004. Late Holocene evolution of the East Eliki Fault, Gulf of Corinth (Central Greece). Quaternary International 115–116, 139–154. doi:10.1016/S1040-6182(03)00103-4.

Peacock, D.C.P., Sanderson, D.J., 1991. Displacements, segment linkage and relay ramps in normal fault zones. Journal of Structural Geology 13, 721–733.

Ramirez-Herrera, M.T., 1998. Geomorphic Assessment of active tectonics in the Acambay Graben, Mexican Volcanic Belt. Earth Surface Processes and Landforms 23, 317–332.

Renz, C., 1955. Die vorneogene Stratigraphie der normal sedimentären Formationen Griechenlands. I.G.S.R., Athens, p. 637.

Roberts, S., Jackson, J.A., 1991. Active normal faulting in central Greece: an overview. In: Roberts, A.M., et al. (Ed.), Geological Society of London, Special Publication, vol. 56, pp. 125–142.

Roberts, G., Koukouvelas, I., 1996. Structural and seismological segmentation of the Gulf of Corinth fault system: implications for models of fault growth. Annali di Geofisica 23, 619–646.

Robertson, A.H.F., Clift, P.D., Degnan, P., Jones, G., 1991. Palaeogeographic and palaeotectonic evolution of the Eastern Mediterranean Neotethys. Palaeogeography, Palaeoclimatology, Palaeoecology 87, 289–344. doi:10.1016/0031-0182(91)90140-M.

Salvany, J.M., 2004. Tilting neotectonics of the Guadiamar Drainage Basin, SW Spain. Earth Surface Processes and Landforms 29, 145–160.

Sboras, S., 2007. Morphotectonic analysis of the neotectonic and active faults of Beotia (Central Greece) with the use of GIS. Master Thesis, Arist. Univ. of Thessaloniki, pp. 185.

Scholz, C.H., Dawers, N.H., Yu, J.J., Anders, M.H., Cowie, P.A., 1993. Fault growth and scaling laws: preliminary results. Journal of Geophysical Research 98, 21,951–21,961.

Silva, P.G., Goy, J.L., Zazo, C., Bardají, T., 2003. Fault-generated mountain fronts in southeast Spain: geomorphologic assessment of tectonic and seismic activity. Geomorphology 50, 203–225.

Smith, A.G., 1977. Othris, Pindos and Vourinos ophiolites and the Pelagonian zone. Proceedings of the 6th Colloquium on the Geology of the Aegean Region, vol. 3. Institute of Geological and Mining Research, Athens, pp. 1369–1374.

Soliva, R., Benedicto, A., 2004. A linkage criterion for segmented normal faults. Journal of Structural Geology 12, 2251–2267.

Tsodoulos, I., Koukouvelas, I., 2004. Faulting and drainage history: the case of Kaparelli Fault, Central Greece. In: Chatzipetros, A.A., Pavlides, S.B. (Eds.), Proceedings of the 5th international Symposium on Eastern Mediterranean Geology, Thessaloniki, Greece, pp. 897–898.

Tsodoulos, I., Koukouvelas, I., 2005. Interaction and linkage of normal faults, examples from Asopia–Kallithea fault zone (Eastern Gulf of Corinth). In: Taymaz, T. (Ed.), Proceedings of International Symposium on the Geodynamics of Eastern Mediterranean: Active Tectonics of the Aegean Region, Istanbul, p. 208.

Walsh, J.J., Bailey, W.R., Childs, C., Nicol, A., Bonson, C.G., 2003. Formation of segmented normal faults: a 3D perspective. Journal of Structural Geology 25, 1251–1262.

Wells, S., Bullard, T., Menges, T., Drake, P., Karas, P., Kelson, K., Ritter, J., Wesling, J., 1988. Regional variations in tectonic geomorphology along segmented convergent plate boundary, Pacific Costa Rica. Geomorphology 1, 239–265.

Yoeli, P., 1965. Analytical hill shading (a cartographic experiment). Surveying and Mapping 25, 573–579.

Zovoili, E., Konstantinidi, E., Koukouvelas, I.K., 2004. Tectonic geomorphology of escarpments: the cases of Kompotades and Nea Anchialos faults. Proceedings of the 10th International Congress. Bulletin of the Geological Society of Greece, Thessaloniki, vol. 36, pp. 1716–1725.

Zuchiewicz, W., 1998. Quaternary tectonics of the Outer West Carpathians, Poland. Tectonophysics 297, 121–132.